

## RESEARCH ARTICLE

# Neuronal deficiency of p38 $\alpha$ -MAPK ameliorates symptoms and pathology of APP or Tau-transgenic Alzheimer's mouse models

Laura Schnöder<sup>1,2</sup> | Gilles Gasparoni<sup>3</sup> | Karl Nordström<sup>3</sup> | Andrea Schottek<sup>1,2</sup> | Inge Tomic<sup>1,2</sup> | Anne Christmann<sup>4</sup> | Karl H. Schäfer<sup>4</sup> | Michael D. Menger<sup>5</sup> | Jörn Walter<sup>3</sup> | Klaus Fassbender<sup>1,2</sup> | Yang Liu<sup>1,2</sup>

<sup>1</sup>Department of Neurology, Saarland University, Homburg, Germany

<sup>2</sup>German Institute for Dementia Prevention (DIDP), Saarland University, Homburg, Germany

<sup>3</sup>Department of Genetics, Saarland University, Saarbrücken, Germany

<sup>4</sup>Working Group Enteric Nervous System, University of Applied Sciences, Zweibrücken, Germany

<sup>5</sup>Department of Experimental Surgery, Saarland University, Homburg, Germany

## Correspondence

Yang Liu, Department of Neurology, Saarland University, Kirrberger Straße, 66421 Homburg/Saar, Germany.  
Email: a.liu@mx.uni-saarland.de

## Funding information

Deutsche Forschungsgemeinschaft (DFG), Grant/Award Number: LI1725/2-1; German federal ministry of research and education, Grant/Award Number: 031L0101D; HOMFORexcell program

## Abstract

Alzheimer's disease (AD) is the leading cause of dementia with very limited therapeutic options. Amyloid  $\beta$  (A $\beta$ ) and phosphorylated Tau (p-Tau) are key pathogenic molecules in AD. P38 $\alpha$ -MAPK is specifically activated in AD lesion sites. However, its effects on AD pathogenesis, especially on p-Tau-associated brain pathology, and the underlying molecular mechanisms remain unclear. We mated human APP-transgenic mice and human P301S Tau-transgenic mice with *mapk14*-floxed and neuron-specific Cre-knock-in mice. We observed that deletion of p38 $\alpha$ -MAPK specifically in neurons improves the cognitive function of both 9-month-old APP and Tau-transgenic AD mice, which is associated with decreased A $\beta$  and p-Tau load in the brain. We further used next-generation sequencing to analyze the gene transcription in brains of p38 $\alpha$ -MAPK deficient and wild-type APP-transgenic mice, which indicated that deletion of p38 $\alpha$ -MAPK regulates the transcription of calcium homeostasis-related genes, especially downregulates the expression of *grin2a*, a gene encoding NMDAR subunit NR2A. Cell culture experiments further verified that deletion of p38 $\alpha$ -MAPK inhibits NMDA-triggered calcium influx and neuronal apoptosis. Our systemic studies of AD pathogenic mechanisms using both APP- and Tau-transgenic mice suggested that deletion of neuronal p38 $\alpha$ -MAPK attenuates AD-associated brain pathology and protects neurons in AD pathogenesis. This study supports p38 $\alpha$ -MAPK as a novel target for AD therapy.

**Abbreviations:** AD, Alzheimer's disease; adcy, adenylate cyclase; AMPA,  $\alpha$ -amino-3-hydroxy-5-methyl-4-isoxazolepropionic acid; APP, Alzheimer's amyloid precursor protein; APP<sup>tg</sup>, human APP-transgenic; APP<sup>wt</sup>, non-APP-transgenic; A $\beta$ , amyloid  $\beta$  peptide; BACE1,  $\beta$ -secretase 1; BDNF, brain-derived neurotrophic factor; C99, C-terminal 99-aminoacid APP fragment; CCL-2, chemokine (C-C motif) ligand 2; Chi3l3, chitinase-like 3; ER, endoplasmic reticulum; ERK, like extracellular signal-related kinases; FA, formic acid; gapdh, glyceraldehyde 3-phosphate dehydrogenase; gnas, guanine nucleotide-binding protein; GO, gene ontology; *gria1*, glutamate ionotropic receptor AMPA type subunit 1; *grin2a*, glutamate ionotropic receptor NMDA type subunit 2A; Iba-1, ionized calcium-binding adapter molecule 1; IGF-1, insulin growth factor 1; IL-1 $\beta$ , interleukin 1 $\beta$ ; iNOS, inducible nitric oxide synthase; JNK, C-Jun N-terminal kinase; LTD, long term depression; LTP, long term potentiation; Mrc1, mannose receptor, C type 1; Munc18-1, Munc18-1 protein mammalian homolog; p38 $\alpha$ -MAPK, p38 mitogen-activated protein kinase type  $\alpha$ ; NeuN, neuronal nuclei; NMDAR, N-methyl-D-aspartate receptors; PSD-95, postsynaptic density protein 95; p-Tau, hyper-phosphorylated Tau; RAB, high-salt reassembly buffer; RIPA, radioimmunoprecipitation assay; RT, room temperature; sec, seconds; sigmar1, sigma non-opioid intracellular receptor1; *slc8a1*, solute carrier family 8 (sodium/calcium exchanger) member; SNAP-25, synaptosome-associated protein 25; Tau<sup>tg</sup>, human Tau-transgenic; Tau<sup>wt</sup>, non-Tau-transgenic; TNF- $\alpha$ , tumor necrosis factor  $\alpha$ .

This is an open access article under the terms of the Creative Commons Attribution-NonCommercial License, which permits use, distribution and reproduction in any medium, provided the original work is properly cited and is not used for commercial purposes.

© 2020 The Authors. *The FASEB Journal* published by Wiley Periodicals LLC on behalf of Federation of American Societies for Experimental Biology

## KEYWORDS

Alzheimer's disease, calcium homeostasis, Mapk14, neurodegeneration, transcriptome analysis

## 1 | INTRODUCTION

Alzheimer's disease (AD) is pathologically characterized by extracellular deposits of amyloid  $\beta$  peptide ( $A\beta$ ) and intracellular neurofibrillary tangles primarily composed of hyperphosphorylated Tau (p-Tau).<sup>1</sup> Growing evidence shows that  $A\beta$  initiates AD pathogenesis: (a)  $A\beta$  aggregates directly injure synaptic junctions and neurons in the neocortex and limbic system,<sup>2</sup> (b) aggregated  $A\beta$  triggers microglia-dominated neurotoxic inflammatory activation,<sup>3</sup> and (c) both  $A\beta$  and neuroinflammation induce phosphorylation of Tau,<sup>4,5</sup> and drive Tau pathology to expand along axonal projections to the entire neocortex.<sup>6,7</sup> Therefore, the reduction of cerebral  $A\beta$  is desirable in AD therapy.

The  $\beta$ -secretase (BACE1) is a speed-limiting enzyme in  $A\beta$  generation from Alzheimer's amyloid precursor protein (APP).<sup>8</sup> Many approaches to inhibit BACE1 have been attempted; unfortunately, these studies have not yet led to efficacious therapy for AD patients.<sup>9</sup> In contrast, the intervention of BACE1 potentially brought severe side effects and even safety problems as BACE1 has various physiological substrates.<sup>10</sup> We recently observed that reduction of p38 $\alpha$ -MAPK, a stress-associated kinase which is highly activated at AD lesion sites in early disease stages,<sup>11,12</sup> facilitated lysosomal degradation of BACE1 in neurons.<sup>13</sup> We argue that inhibition of p38 $\alpha$ -MAPK might be an alternative method to block BACE1-mediated  $A\beta$  production. Moreover, deficiency of p38 $\alpha$ -MAPK reduces  $A\beta$ -triggered inflammatory activation in cultured microglia.<sup>14</sup> p38-MAPK has been shown to phosphorylate recombinant Tau protein,<sup>15</sup> and has been observed to bind p-Tau in the AD brain.<sup>12,16</sup> There is also evidence that p38-MAPK might mediate  $A\beta$ -induced synaptic impairment.<sup>17,18</sup> An exploratory clinical study on p38 $\alpha$ -MAPK inhibitor did show a promising result that p38 $\alpha$ -MAPK inhibition might improve episodic memory and impact amyloid deposits in AD patients.<sup>19</sup> Thus, it is worthwhile to extensively investigate the pathophysiological role of p38 $\alpha$ -MAPK in AD.

Administration of p38 $\alpha$ -MAPK inhibitor in both APP- and Tau-transgenic AD mice suppresses inflammatory activation and attenuates neuronal deficits in the brain.<sup>20-22</sup> However, pharmacological experiments are not able to distinguish the effect from neuronal and microglial p38 $\alpha$ -MAPK. Deletion of p38 $\alpha$ -MAPK specifically in neurons reduced cerebral  $A\beta$  and BACE1 proteins in 5XFAD mice,<sup>23</sup> which corroborates our previous finding.<sup>13</sup> However, this study did not further decode the underlying mechanisms mediating neuronal protection. Moreover, most preclinical studies on p38 $\alpha$ -MAPK have used APP-transgenic mice

as AD models and neglected the effects of p38 $\alpha$ -MAPK on p-Tau-associated pathology, which prevent comprehensively understanding the pathogenic role of p38 $\alpha$ -MAPK in AD.

To address these questions, we deleted p38 $\alpha$ -MAPK in neurons of both APP- and Tau-transgenic mice and observed that deletion of neuronal p38 $\alpha$ -MAPK attenuated cognitive dysfunctions in association with decreased loads of  $A\beta$  and p-Tau, and inhibited inflammatory activation in the brain. We further compared the transcriptome in brains from neuronal p38 $\alpha$ -MAPK-deficient and wild-type APP-transgenic mice, and showed that deletion of p38 $\alpha$ -MAPK might regulate neuronal calcium homeostasis and protect neurons in AD.

## 2 | MATERIALS AND METHODS

## 2.1 | Animal models and cross-breeding

Our APP-transgenic (APP<sup>tg</sup>) mice over-expressing human mutated APP (KM670/671NL) and presenilin-1 (L166P) under Thy-1 promoters<sup>24</sup> were kindly provided by M. Jucker, Hertie Institute for Clinical Brain Research, Tübingen; p38<sup>fl/fl</sup> mice carrying loxP site-flanked *mapk14* gene were provided by K. Otsu, Osaka University;<sup>25</sup> and K. Nave, Max-Planck-Institute for Medicine, Göttingen, kindly provided Nex-Cre mice, expressing Cre recombinase from the endogenous locus of *nex* gene.<sup>26</sup> APP<sup>tg</sup>, p38<sup>fl/fl</sup>, and Nex-Cre mice, all on a C57BL6 genetic background, had been cross-bred in our previous study to build AD animal models with (APP<sup>tg</sup>p38<sup>fl/fl</sup>Cre<sup>+/-</sup>) and without (APP<sup>tg</sup>p38<sup>fl/fl</sup>Cre<sup>-/-</sup>) deletion of p38 $\alpha$ -MAPK in neurons.<sup>13</sup> In order to investigate physiological function of p38 $\alpha$ -MAPK in neurons, we also examined non-APP-transgenic (APP<sup>wt</sup>) mice with (APP<sup>wt</sup>p38<sup>fl/fl</sup>Cre<sup>+/-</sup>) and without (APP<sup>wt</sup>p38<sup>fl/fl</sup>Cre<sup>-/-</sup>) deletion of neuronal p38 $\alpha$ -MAPK. To evaluate the effect of neuronal p38 $\alpha$ -MAPK on p-Tau-induced phenotype, we cross-bred p38<sup>fl/fl</sup> and Nex-Cre mice, with P301S Tau-transgenic (Tau<sup>tg</sup>) mice (imported from the Jackson Laboratory, Bar Harbor, MA, USA; Stock: #008169), which over-express the human Tau mutant (P301S) under the direction of mouse prion protein promoter.<sup>27</sup> For this study, 9-month-old male and female mice were used. All animal experiments were performed in accordance with relevant national rules and authorized by the local research ethical committee (permission numbers: 40/2014 and 49/2016).

## 2.2 | Morris water maze

The Morris water maze test, consisting of a 6-day training phase and a 1-day probe trial, was used to assess the cognitive function of APP<sup>tg</sup> or Tau<sup>tg</sup> mice and their APP<sup>wt</sup> littermates, as previously described.<sup>28</sup>

## 2.3 | Tissue collection for histological and biochemical analysis

Animals were euthanized by inhalation of isoflurane. The brain was removed and divided. The left hemisphere was immediately fixed in 4% paraformaldehyde (Sigma-Aldrich GmbH, Taufkirchen, Germany) and embedded in paraffin. A 0.5- $\mu$ m-thick piece of tissue was sagittal cut from the right hemisphere. The cortex and hippocampus were separated and homogenized in TRIzol (Thermo Fisher Scientific, Darmstadt, Germany) for RNA isolation. The remainder of the right hemisphere was snap-frozen in liquid nitrogen and stored at  $-80^{\circ}\text{C}$  until biochemical analysis. To evaluate the activity of p38-MAPK, we also collected heart, left lobe of liver, and skeletal muscles of quadriceps.

## 2.4 | Western blot analysis

Frozen mouse brains were homogenized on ice in radioimmunoprecipitation assay buffer (RIPA buffer; 50 mM Tris [pH 8.0], 150 mM NaCl, 0.1% SDS, 0.5% sodiumdeoxycholate, 1% NP-40, and 5 mM EDTA) supplemented with protease inhibitor cocktail (Roche Applied Science, Mannheim,

Germany) and phosphatase inhibitors (50 nM okadaic acid, 5 mM sodium pyrophosphate, and 50 mM NaF; Sigma-Aldrich). To quantify p-Tau and total Tau (t-Tau) proteins, the brain tissue was sequentially homogenized in ice-cold high-salt reassembly buffer (RAB; 0.1 M MES, 1 mM EGTA, 0.5 mM MgSO<sub>4</sub>, 0.75 M NaCl, 20 mM NaF, and 1 mM PMSF), RIPA buffer, and 70% formic acid (FA).<sup>28</sup> Human A $\beta$ , Tau, and other brain proteins were quantified with previously established Western blot<sup>13,28</sup> using antibodies listed in Table 1.

## 2.5 | Golgi - Cox staining

Serial 100- $\mu$ m-thick sagittal sections were cut from mouse brains using a vibratome (VT1000S, Leica Mikrosysteme Vertrieb GmbH, Wetzlar, Germany) and stained with Rapid Golgi Staining Kit (FD NeuroTechnologies, Columbia, MA, USA). Images of neurons at hippocampal CA1 and CA3 and at cortex (layer II/III) were obtained on a Zeiss AxioImager.Z2 microscope with a 63 $\times$  oil-objective and a z-stack distance of 0.5  $\mu$ m (Zeiss Microscopy, Göttingen, Germany). The number of spines per micrometer of dendritic length was determined in second- or third-order dendritic branches of apical dendrites. At minimum, three serial sections per animals with 500  $\mu$ m of interval were analyzed. Moreover, the morphology of dendritic spines were analyzed and spines were grouped into mature (mushroom), immature (thin and stubby), and filopodia-like spines according to the published classification.<sup>29</sup> The experimenter was blinded to the genotypes of mice during the entire experiment.

**TABLE 1** List of antibodies used for quantitative Western blot

Antibodies	Supplier	Species	Type	Reference
p38-MAPK	Cell Signaling Technology	Rabbit	Polyclonal	Catalog no. 9212
phosphorylated p38-MAPK	Cell Signaling Technology	Rabbit	Polyclonal	Catalog no. 9211
PSD-95	Cell Signaling Technology	Rabbit	Polyclonal	Catalog no. 2507
SNAP-25	Cell Signaling Technology	Rabbit	Polyclonal	Catalog no. 3926
Munc18-1	Cell Signaling Technology	Rabbit	Polyclonal	Catalog no. 13414
synaptophysin	Abcam	Mouse	Monoclonal	Clone SY38
A $\beta$	Merck Chemicals GmbH	Mouse	Monoclonal	Clone W0-2
Tau	Thermo Fisher Scientific	Mouse	Monoclonal	Clone HT7
Phosphorylated Tau	Thermo Fisher Scientific	Mouse	Monoclonal	Clone AT8
Grin2a	Cell Signaling Technology	Rabbit	Polyclonal	Catalog no. 4205
$\beta$ -actin	Cell Signaling Technology	Rabbit	Monoclonal	Clone 13E5
$\alpha$ -tubulin	Abcam	Mouse	Monoclonal	Clone DM1A
LC3B	Cell Signaling Technology	Rabbit	monoclonal	Clone D11
Cleaved Caspase-3	Cell Signaling Technology	Rabbit	Monoclonal	Clone 5A1E

## 2.6 | Immunohistological analysis

Serial 50- $\mu\text{m}$ -thick sagittal sections were cut from the paraffin-embedded hemisphere. Human A $\beta$  in APP<sup>tg</sup> mouse brains was stained with mouse anti-human A $\beta$  antibody (clone 6F/3D; Dako Deutschland GmbH, Hamburg, Germany) and microglia labeled with rabbit anti-ionized calcium-binding adapter molecule (Iba)-1 antibody (Wako Chemicals, Neuss, Germany). For each animal we labeled four sections with an interval of 10 layers between neighbouring sagittal sections. In the whole hippocampus and cortex, volumes of A $\beta$  were estimated with the Cavalieri method, and Iba-1-positive cells were counted with Optical Fractionator as described previously<sup>30</sup> on a Zeiss AxioImager.Z2 microscope equipped with a Stereo Investigator system (MBF Bioscience, Williston, VT, USA).

To evaluate Tau pathology in Tau<sup>tg</sup> mice, four serial 50- $\mu\text{m}$ -thick sections were chosen as for A $\beta$  analysis. Brain tissues were stained according to the published protocols<sup>31</sup> with a mouse monoclonal antibody against human phospho-Tau (Ser202, Thr205) (clone: AT8; Thermo Fisher Scientific) or with thioflavine S (Sigma-Aldrich GmbH). Thioflavine S staining was used to identify neurofibrillary tangles. Because of low numbers of p-Tau or thioflavine S staining-positive cells in the cortex and hippocampus, we did not use stereological analysis, but counted labeled cells in the whole brain region. Data were recorded as the number of labeled cells divided by the full area (in square millimeters) of interest.

To evaluate the efficiency and specificity of Nex-Cre-mediated deletion of p38 $\alpha$ -MAPK, we co-stained brain sections from 9-month-old APP<sup>tg</sup>p38 $\alpha^{\text{fl/fl}}$ Cre<sup>+/-</sup> and APP<sup>tg</sup>p38 $\alpha^{\text{fl/fl}}$ Cre<sup>-/-</sup> mice with antibodies against NeuN (clone: D4G40; Cell Signaling Technology, Frankfurt am Main, Germany), and p38 $\alpha$ -MAPK (clone: 9F12; Novus Biologicals, Wiesbaden, Germany), and then, with Alexa Fluor 488 and CY3-conjugated secondary antibodies, respectively. Nuclei were counterstained with DAPI. We randomly chose cortical regions under 40 $\times$  objective. In the channels for Alexa Fluor 488 and DAPI fluorescence, we first counted NeuN-positive and negative cells with clear nuclear staining. Thereafter, we imaged sections in the channel for CY3 to count p38 $\alpha$ -MAPK-staining positive cells. More than 800 NeuN-positive cells and >400 NeuN-negative cells were counted and the percentages of p38 $\alpha$ -MAPK-positive cells within these two groups of cells were calculated.

## 2.7 | Quantitative PCR for analysis of gene transcripts

Total RNA was isolated from mouse brains and reverse transcribed. Gene transcripts of pro- and anti-inflammatory

markers were quantified with our established protocol<sup>30</sup> using Taqman gene expression assays of mouse *tnf- $\alpha$* , *il-1 $\beta$* , *chemokine (C-C motif) ligand 2 (ccl-2)*, *inducible nitric oxide synthase (inos)*, *il-10*, *arginase 1 (arg1)*, *mannose receptor C type 1 (mrc1)*, *chitinase-like 3 (chi3l3)*, *brain-derived neurotrophic factor (bdnf)*, *insulin growth factor (igf)-1*, and *glyceraldehyde 3-phosphate dehydrogenase (gapdh)* (Thermo Fisher Scientific). After next generation sequencing analysis, the transcription of following target genes encoding: *adenylate cyclase 3 and 7 (adcy3, adcy7)*, *ATPase plasma membrane Ca<sup>2+</sup> transporting 4 (atp2b4)*, *guanine nucleotide-binding protein (gnas)*, *grin2a*, *5-hydroxytryptamine receptor 7 (htr7)*, *solute carrier family 8 (sodium/calcium exchanger), member 1 (slc8a1)*, *sphingosine kinase 1 (sphk1)*, *transmembrane protein 63C (tmem63c)*, *phosphoinositide-specific phospholipase C (plch1)*, and *nuclear factor of activated T cells 2 (nfatc2)*, was determined using SYBR green binding technique with primers shown in Table 2. For *nfatc2* detection, two different sets of primers for transcript variants were used.

## 2.8 | RNA purification for next generation sequencing

RNA from 9-month-old p38 $\alpha$ -MAPK-deficient and wild-type APP<sup>tg</sup> littermate mice was purified using the RNeasy Plus Mini Kit (Qiagen GmbH, Hilden, Germany) according to the manufacturer's instructions. The concentration and integrity of RNA were tested using the Agilent 2100 Bioanalyzer (Santa Clara, CA, USA). RNA samples with RNA integrity number > 6 were used to build RNA-sequencing libraries.

## 2.9 | Preparation of RNA-sequencing library

The RNA-seq library was built with 600 ng total RNA using the NEBNext Poly(A) mRNA Magnetic Isolation Module (Ipswich), NEBNext Ultra Directional RNA Library Prep Kit for Illumina (E7420) and NEBNext Multiplex Oligos for Illumina (Index-Set2) (New England Biolabs GmbH, Frankfurt am Main, Germany). Briefly, mRNA was enriched using AMPure XP Beads (Beckman Coulter GmbH, Krefeld, Germany), fragmented using enzymes, and then, reverse transcribed into cDNA with random primers. Thereafter, double stranded cDNA was adaptor-ligated and amplified by PCR for 10 cycles. The quality of libraries was evaluated using the High Sensitivity DNA Chip in the Agilent 2001 Bioanalyzer and quantified by qPCR with the PerfeCTa NGS quantification kit from QuantaBio (Beverly, MA, USA).

Gene	Sense	Antisense
Adcy3	AGCTTGTGGCCTTCTCATCT	CCATCCCAGCTGTCATGTTG
Adyc7	ACATGCCACTGACGCTTAAC	TTCAGCTCTAGGCTCATCCG
Atp2b4	CCCTGCAGATTGGAGAAGC	GAGGTCCGGTAGAAGGACAGG
GAPDH	ACAACCTTGGCATTGTGGAA	GATGCAGGGATGATGTTCTG
Gnas	GACTGTGCCAGTACTTCCT	TCCACCTGGAACCTTGGTCTC
Grin2a	CCATCTTGGGCATTCATGGG	AGATGGTGGTGACCAAGGAG
HTR7	GCAAGGCCCTTATCTGTGG	GCACTGGAGTAGGCTACGAT
Nfatc2_1207	CTGGGCAGAATTCTCGTGTG	GGCATTGCTCCAGTCAGAAG
Nfatc2_4293	CGCCACATCTACCCTACTGT	ATAGGAGCCCGACTGATTGG
Plch1	GCAAAGTGGGCTTCCAAGAA	GCATAGAGACAGGGCGTACT
Slc8a1	TAGGCCCTTTCATCACAGCA	AAGCAAATTCAGCCTGCCAA
Sphk1	GAGCCAGTGCCTTCTCATTG	GCATAACACCAGCCTCACAG
Tmem63c	TCAGCTCCTCGTTCCAACCT	ATGGGTGGAGACACTTGGAG

**TABLE 2** List of primer sequences used for SYBR green based quantitative RT-PCR

## 2.10 | Illumina Sequencing and Sequence alignment

The libraries were sequenced on the Illumina HiSeq2500 platform (San Diego, CA, USA) with 101-bp single-end reads. After QC with FastQC Version 0.11.2 (<http://www.bioinformatics.bbsrc.ac.uk/projects/fastqc/>), reads were adaptor-trimmed ( $Q < 20$ ) with Cutadapt (Version 1.4.1<sup>32</sup>) with a wrapper Trim Galore! (Version 0.3.3) ([https://www.bioinformatics.babraham.ac.uk/projects/trim\\_galore/](https://www.bioinformatics.babraham.ac.uk/projects/trim_galore/)). Reads were aligned with the grape-nf pipeline (<https://github.com/guigolab/grape-nf>) wrapping STAR (Version 2.4.0j<sup>33</sup>) and RSEM (Version 1.2.21<sup>34</sup>). Read counts were imported into R with tximport (Version 1.6.0<sup>35</sup>). Differentially expressed genes were identified with edgeR (Version 3.20.9<sup>36</sup>). Transcripts with an absolute log<sub>2</sub>-fold change greater than 2 and a FDR value below 0.01 were considered differentially expressed.

## 2.11 | Gene ontology (GO) and pathway analysis

The biological function of individual genes was identified by GO analysis (<http://cbl-gorilla.cs.technion.ac.il/>). KEGG pathways with high gene transcript clustering were processed and downloaded using the online software Pathview.<sup>37-39</sup>

## 2.12 | Culture of primary neurons

Cortex was collected from embryos (E14 ± 0.5) from the breeding of APP<sup>tg</sup>p38<sup>fl/fl</sup>Nex-Cre<sup>+/-</sup> (or APP<sup>wt</sup>p38<sup>fl/fl</sup>Nex-Cre<sup>+/-</sup>) male and APP<sup>wt</sup>p38<sup>fl/fl</sup>Nex-Cre<sup>-/-</sup> female mice. After digestion with trypsin for 15 minutes at 37°C, the single cell

suspension ( $2 \times 10^5$  cells) was seeded on a poly-L-lysine-coated coverslip with 15 mm of diameter. Primary neurons were cultured for  $14 \pm 2$  days at 37°C and 10% CO<sub>2</sub> in neurobasal medium supplemented with 2% B27, 0.25% L-Glutamine, and 0.1% Glutamax (all reagents were bought from Thermo Fisher Scientific).

## 2.13 | Calcium imaging of primary neurons

The functional analysis of altered calcium homeostasis was evaluated by calcium imaging. We incubated the neurons with 5 μM Fluo-4 (Thermo Fisher Scientific) for 30 minutes at RT. After washing, we aligned the coverslip in a perfusion chamber RC-20 (Warner Instruments, Hamden, CT, USA) and applied a constant perfusion (0.5 mL/min) with imaging buffer (148 mM NaCl, 5 mM KCl, 2 mM CaCl<sub>2</sub>, 1 mM MgCl<sub>2</sub>, 10 mM Glucose, 10 mM HEPES [pH 7.38]). Calcium images were taken with an inverse Olympus microscope (IX-70; Olympus Deutschland GmbH, Hamburg, Germany), equipped with a 20× objective (Olympus) and a CCD camera (Orca-II-ER; Hamamatsu Photonics Deutschland GmbH, Herrsching am Ammersee, Germany). The basal activity of neurons was detected for 90 seconds. Then, the neurons of both genotypes were stimulated with either 100 μM L-glutamate or 50 μM NMDA (both from Sigma-Aldrich) in imaging buffer. When the calcium response reached a plateau, 500 μM L-glutamate (at 400 seconds) or 10 mM NMDA (at 300 seconds) was further administered to neurons. As a control, 75 mM KCl was used to stimulate neurons. Images were processed and analyzed with the software CellObserver Z1 and Axiovision (Zeiss Microscopy, Göttingen, Germany). Region of interests were set around the fluorescent neuronal cell bodies. The ratio  $F/F_0$  was calculated (F: fluorescent intensity at different time points,  $F_0$ : basal fluorescent intensity

at the time point 0). Calcium influx ( $\Delta\text{Ca}^{2+}$ ) =  $(F-F_0)/F_0$ . Four independent experiments were performed for each stimulator. The mean value of  $\Delta\text{Ca}^{2+}$  from all analyzed cells on the same coverslip was calculated for each animal.

To evaluate intracellular calcium buffering capacity, we stimulated p38 $\alpha$ -MAPK-deficient and wild-type neurons with 100  $\mu\text{M}$  L-glutamate for 20 seconds after 60 seconds of baseline acquisition. Thereafter, a constant perfusion (0.5 mL/min) with imaging buffer was applied to the chamber to wash out L-glutamate for around 180 seconds (until the fluorescence intensity returned to the baseline level). The time during which the intensity of Fluo-4 fluorescence went back to the baseline after wash-out was calculated as decay time (see Figure 6F).

To investigate the effects of p38 $\alpha$ -MAPK deletion on calcium influx after blocking NMDAR, we continued to perfuse p38 $\alpha$ -MAPK-deficient and wild-type neurons from the wash-out experiment (described above) constantly with imaging buffer containing 100  $\mu\text{M}$  NMDAR antagonist, 2-APV (Tocris Bioscience, Wiesbaden-Nordenstadt, Germany; Cat. No.: 0106) at 0.5 mL/min for 300 seconds. Thereafter, neurons were again stimulated with 100  $\mu\text{M}$  L-glutamate for 20 seconds in presence of 100  $\mu\text{M}$  2-APV. After a further 180-sec treatment with 100  $\mu\text{M}$  2-APV, neurons were washed with pure imaging buffer (see Figure 6F).

In all calcium imaging experiments, the experimenter was blinded to the genotypes of cells.

## 2.14 | Apoptosis assay of p38 $\alpha$ -MAPK-deficient and wild-type primary neurons

To evaluate the effects of p38 $\alpha$ -MAPK deficiency on calcium influx-induced neuronal death, we treated cultured p38 $\alpha$ -MAPK-deficient and wild-type neurons with 100  $\mu\text{M}$  L-glutamate or 50  $\mu\text{M}$  NMDA for 16 hours. Thereafter, neurons were harvested and lysed in RIPA buffer. Quantitative Western blot was used to detect caspase-3 activity in the cell lysate with antibodies specifically against cleaved caspase-3 (Clone 5A1E; Cell Signaling Technology). This antibody detects cleaved (active) caspase-3 without showing pro-caspase-3.

## 2.15 | Statistics

Data were presented as mean  $\pm$  SEM. For multiple comparisons, one-way or two-way ANOVA followed by Bonferroni, Tukey, or Dunnett T3 post hoc test (dependent on the result of Levene's test to determine the equality of variances) was used. Two independent-samples Students *t* test was used to compare means for two groups of cases. All statistical analyses were performed with SPSS version 19.0 for Windows

(IBM, New York, NY, USA). Statistical significance was set at  $P < .05$ .

## 3 | RESULTS

### 3.1 | Determination of lesion sites-associated activation of p38-MAPK in APP-transgenic mice and establishment of neuronal p38 $\alpha$ -MAPK-deficient AD mouse models

Based on previous reports showing that p38-MAPK is activated in association with AD pathological changes,<sup>6,11,12,40</sup> we hypothesized that phosphorylation of p38-MAPK would be greater in APP<sup>tg</sup> mice compared to non-APP-transgenic (APP<sup>wt</sup>) animals. We measured p38-MAPK activities in brain, heart, muscles, and liver of 9-month-old APP<sup>tg</sup> and APP<sup>wt</sup> littermates. The results showed that phosphorylation of p38-MAPK was increased in the brain of the APP<sup>tg</sup> mice, compared to the APP<sup>wt</sup> littermates, but not in the other organs tested (Figure 1A,B; *t* test,  $P = .025$ ), confirming that p38-MAPK is activated in association with AD lesions.

To verify the deletion of p38 $\alpha$ -MAPK in the brain, we measured the cerebral protein levels of p38-MAPK in 9-month-old APP<sup>tg</sup>p38 $\alpha$ <sup>fl/fl</sup>Cre<sup>+/-</sup> and APP<sup>tg</sup>p38 $\alpha$ <sup>fl/fl</sup>Cre<sup>-/-</sup> littermate mice and found the levels of p38-MAPK to be 75% lower in Cre-positive mice compared to Cre-negative littermates (Figure 1C,D; p38-MAPK/ $\alpha$ -tubulin:  $0.245 \pm 0.036$  vs  $1.005 \pm 0.162$ , respectively; *t* test,  $P = .003$ ).

We then co-stained p38 $\alpha$ -MAPK and NeuN, a neuronal marker, in brains of 9-month-old APP<sup>tg</sup>p38 $\alpha$ <sup>fl/fl</sup>Cre<sup>+/-</sup> and APP<sup>tg</sup>p38 $\alpha$ <sup>fl/fl</sup>Cre<sup>-/-</sup> littermates. In the cortex of APP<sup>tg</sup>p38 $\alpha$ <sup>fl/fl</sup>Cre<sup>-/-</sup> mice, p38 $\alpha$ -MAPK protein was stained and shown in puncta around the nucleus in  $48.67 \pm 6.95\%$  NeuN antibody-stained cells (Figure 1E), whereas, only  $12.81 \pm 3.86\%$  NeuN-positive cells in APP<sup>tg</sup>p38 $\alpha$ <sup>fl/fl</sup>Cre<sup>+/-</sup> mice showed p38 $\alpha$ -MAPK signals (Figure 1F; *t* test,  $P < .001$ ). In NeuN-negative brain cells, the staining of p38 $\alpha$ -MAPK was not different between these two groups of AD mice (Figure 1F;  $21.39 \pm 4.85\%$  vs  $19.59 \pm 4.06\%$ , in APP<sup>tg</sup>p38 $\alpha$ <sup>fl/fl</sup>Cre<sup>+/-</sup> and APP<sup>tg</sup>p38 $\alpha$ <sup>fl/fl</sup>Cre<sup>-/-</sup> mice, respectively; *t* test,  $P > .05$ ). The cellular specificity of Cre-mediated p38 $\alpha$ -MAPK deletion in neurons of APP<sup>tg</sup> mice corroborates our previous observation.<sup>13</sup>

Interestingly, in the additional experiments, we observed that deletion of p38 $\alpha$ -MAPK was able to further inhibit phosphorylation of the rest of p38-MAPK protein in p38 $\alpha$ -MAPK-deficient APP<sup>tg</sup> mouse brain but not in p38 $\alpha$ -MAPK-deficient APP<sup>wt</sup> mice (Figure 1G,H; one-way ANOVA,  $P < .05$ ).

In our study, we produced a total of 361 new-born mice from the following two breeding pairs: (a) APP<sup>tg</sup>p38 $\alpha$ <sup>fl/fl</sup>Cre<sup>+/-</sup> [male] and APP<sup>wt</sup>p38 $\alpha$ <sup>fl/fl</sup>Cre<sup>-/-</sup> [female], and (b) APP<sup>tg</sup>p38 $\alpha$ <sup>fl/fl</sup>Cre<sup>-/-</sup> [male] and APP<sup>wt</sup>p38 $\alpha$ <sup>fl/fl</sup>

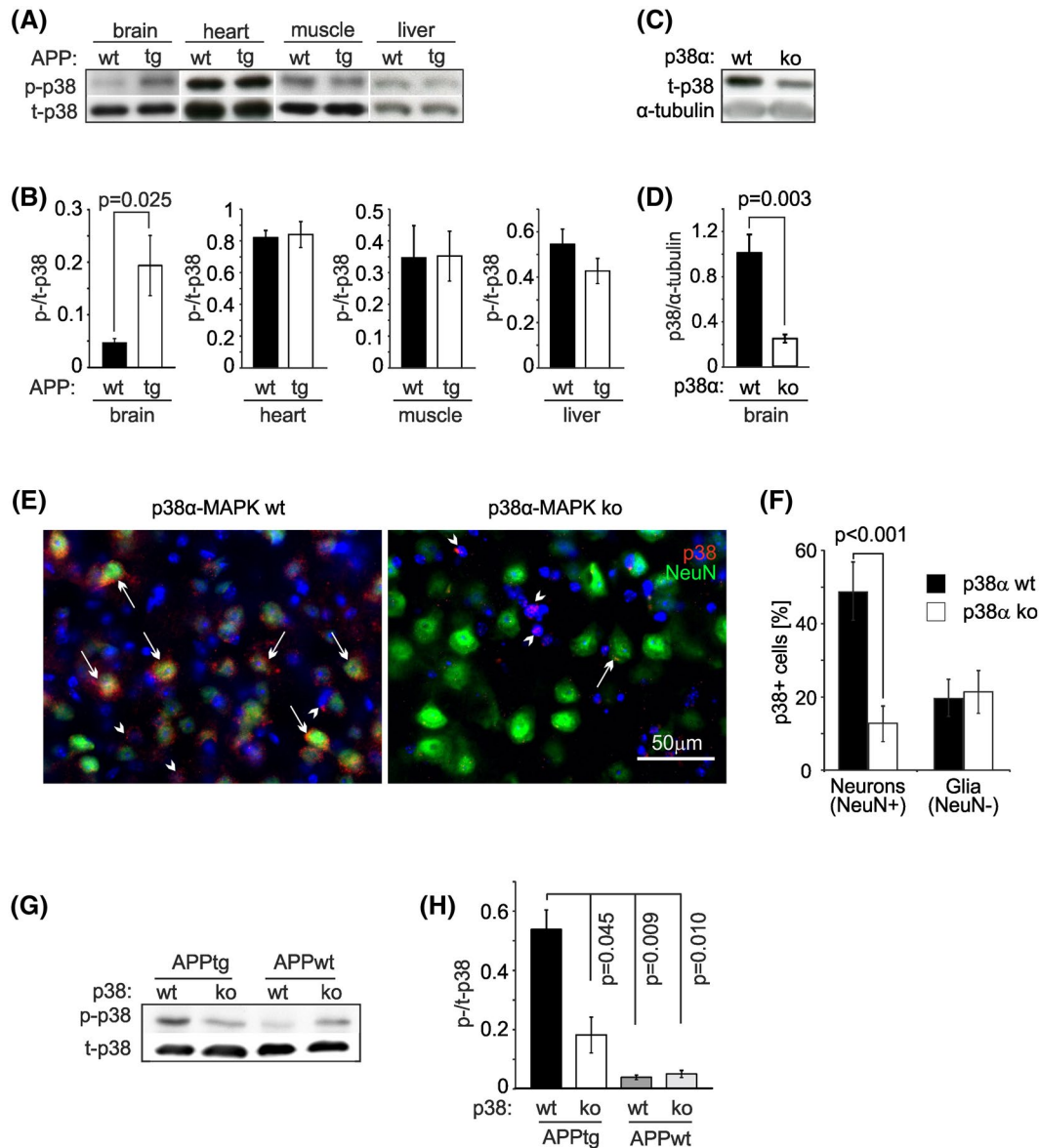


**FIGURE 1** p38-MAPK is activated in APP-transgenic mouse brain and is efficiently deleted in neurons of  $APP^{tg}p38^{fl/fl}Cre^{+/-}$  mice. The homogenates of brain, heart, muscle, and liver derived from 9-month-old APP-transgenic ( $APP^{tg}$ ) and wild-type ( $APP^{wt}$ ) littermates were analyzed for both phosphorylated (p-p38) and total (t-p38) p38-MAPK with Western blot (A and B, *t* test,  $n \geq 4$  per group). Western blot was also used to detect cerebral t-p38 in 9-month-old  $APP^{tg}p38^{fl/fl}Cre^{+/-}$  (p38 $\alpha$ -MAPK-ko) and  $APP^{tg}p38^{fl/fl}Cre^{-/-}$  (p38 $\alpha$ -MAPK-wt) littermate mice (C and D, *t* test,  $n = 5$  per group). Brain sections of these mice were co-stained with fluorophore-conjugated antibodies against p38 $\alpha$ -MAPK and NeuN in the cortex (E). In p38 $\alpha$ -MAPK-wt mice, p38 $\alpha$ -MAPK protein was shown in red puncta around the NeuN-staining nuclei in green (indicated with arrows), whereas, rare p38 $\alpha$ -MAPK was stained in NeuN staining-positive neurons in p38 $\alpha$ -MAPK-ko mice. In NeuN staining-negative cells, p38 $\alpha$ -MAPK was stained in both p38 $\alpha$ -MAPK-wt and ko mice (E, indicated with arrow heads). Nuclei were stained with DAPI in blue. The percentages of p38 $\alpha$ -MAPK-stained cells in both NeuN-positive and negative cells were calculated and compared in p38 $\alpha$ -MAPK-wt and ko  $APP^{tg}$  mice (F, *t* test,  $n = 11$  per group). The homogenates of brain derived from 9-month-old  $APP^{wt}$  and  $APP^{tg}$  littermates with and without deletion of p38 $\alpha$ -MAPK were further analyzed for phosphorylation of p38-MAPK with quantitative Western blot. In this experiment, the loading protein for each lane was adapted to have similar amount of t-p38 (G and H, One-Way ANOVA followed by Bonferroni post hoc test,  $n \geq 4$  per group)

$flCre^{+/-}$  [female]. The genotypes (percentages) of the newborn mice were  $APP^{wt}p38^{fl/fl}Cre^{-/-}$  (19.11%),  $APP^{wt}p38^{fl/fl}Cre^{+/-}$  (30.75%),  $APP^{tg}p38^{fl/fl}Cre^{-/-}$  (22.44%), and  $APP^{tg}p38^{fl/fl}Cre^{+/-}$  (27.70%), as shown in Table 3 ( $\chi^2$  test

between different genotypes,  $P = .984$ ). Mice with deletion of p38 $\alpha$ -MAPK appeared to be generally healthy, fertile, and behaviorally normal, demonstrating that deletion of neuronal p38 $\alpha$ -MAPK is not toxic to the survival of mice.

**TABLE 3** Genotype distribution of newborns from the following two breeding pairs: (i)  $app^{tg}p38\alpha^{fl/fl}Cre^{+/-}$  [male] and  $app^{wt}p38\alpha^{fl/fl}Cre^{-/-}$  [female]; and (ii)  $app^{tg}p38\alpha^{fl/fl}Cre^{-/-}$  [male] and  $app^{wt}p38\alpha^{fl/fl}Cre^{+/-}$  [female]

	$app^{wt}p38\alpha^{fl/fl}Cre^{-/-}$	$app^{wt}p38\alpha^{fl/fl}Cre^{+/-}$	$app^{tg}p38\alpha^{fl/fl}Cre^{-/-}$	$app^{tg}p38\alpha^{fl/fl}Cre^{+/-}$	Total
Male	34 (33.8)	53 (54.4)	41 (39.7)	49 (49.0)	177 (177.0)
Female	35 (35.2)	58 (56.6)	40 (41.3)	51 (51.0)	184 (184.0)
Total	69 (69.0)	111 (111.0)	81 (81.0)	100 (100.0)	361 (361.0)

Note: Values in brackets indicate the expected counts from  $\chi^2$  test.

$\chi^2 = 0.156$ ,  $F = 3$  and  $P = .984$ .

### 3.2 | Deletion of neuronal p38 $\alpha$ -MAPK attenuates cognitive deficits and synaptic impairments in APP-transgenic mice

In order to test the pathogenic effects of neuronal p38 $\alpha$ -MAPK on AD, we used the Morris water maze test to examine the cognitive function of 9-month-old APP<sup>tg</sup> and APP<sup>wt</sup> littermate mice with and without deletion of p38 $\alpha$ -MAPK in neurons. As shown in Figure 2A-C, the swimming time and distance to reach the platform for all tested mice significantly decreased when the training time increased (two-way ANOVA,  $P < .05$ ); however, the swimming velocity did not differ between various groups of mice or for the same mice on different training dates (two-way ANOVA,  $P > .05$ ).

We compared different genotypes of mice with respect to their behavior during the acquisition phase of the water maze test. APP<sup>wt</sup> littermate mice with or without deficiency of p38 $\alpha$ -MAPK in neurons ( $APP^{wt}p38\alpha^{fl/fl}Cre^{+/-}$  and  $APP^{wt}p38\alpha^{fl/fl}Cre^{-/-}$ ) showed no significant differences in either swimming time or swimming distance before climbing onto the escape platform (Figure 2A,B; two-way ANOVA,  $P > .05$ ). Compared to  $APP^{wt}p38\alpha^{fl/fl}Cre^{+/-}$  or  $APP^{wt}p38\alpha^{fl/fl}Cre^{-/-}$  littermates, 9-month-old APP<sup>tg</sup> mice with wild-type p38 $\alpha$ -MAPK expression in neurons ( $APP^{tg}p38\alpha^{fl/fl}Cre^{-/-}$ ) spent significantly more time (Figure 2A; two-way ANOVA,  $P < .05$ ) and traveled longer distances (Figure 2B; two-way ANOVA,  $P < .05$ ) in the water maze before reaching the escape platform. Interestingly,  $APP^{tg}p38\alpha^{fl/fl}Cre^{+/-}$  mice with the ablation of p38 $\alpha$ -MAPK specifically in neurons performed significantly better than their  $APP^{tg}p38\alpha^{fl/fl}Cre^{-/-}$  littermates in searching for and finding the platform after 3 days of training (Figure 2A,B; two-way ANOVA followed by post hoc test showing  $APP^{tg}p38\alpha^{fl/fl}Cre^{-/-}$  vs  $APP^{tg}p38\alpha^{fl/fl}Cre^{+/-}$  mice:  $P < .05$ ).

Twenty-four hours after the end of the training phase, the escape platform was removed and a 5-minute probe trial was performed to test the memory of the mice. We evaluated three parameters: duration of time the mouse needed to find the original platform region, total number of times the mouse crossed the original platform region, and the total time the mouse spent in the original platform region. Compared to  $APP^{wt}p38\alpha^{fl/fl}Cre^{+/-}$  and  $APP^{wt}p38\alpha^{fl/fl}Cre^{-/-}$  littermates,  $APP^{tg}p38\alpha^{fl/fl}Cre^{-/-}$  mice took significantly longer time for

their first visit to the region where the platform had been located, crossed the platform region with significantly less frequency, and spent significantly less time in the platform region during the total 5-minute probe trial (Figure 2D-F; one-way ANOVA followed by post hoc test,  $P < .01$ ). Interestingly, when compared to  $APP^{tg}p38\alpha^{fl/fl}Cre^{-/-}$  mice,  $APP^{tg}p38\alpha^{fl/fl}Cre^{+/-}$  mice were able to reach the original platform region in significantly less time and crossed the region more frequently (Figure 2D,E; one-way ANOVA followed by post hoc test,  $P = .03$  and  $0.05$ , respectively). We observed no significant differences between the two  $APP^{wt}$  control groups ( $APP^{wt}p38\alpha^{fl/fl}Cre^{+/-}$  and  $APP^{wt}p38\alpha^{fl/fl}Cre^{-/-}$  littermate mice) in any of the three parameters analyzed in the probe trial (Figure 2D-F; one-way ANOVA followed by post hoc test,  $P > .05$ ).

We also used Western blot analysis to quantify the levels of four synaptic-structure proteins: Munc18-1, synaptophysin, SNAP-25, and PSD-95 in the brain homogenate of 9-month-old APP<sup>tg</sup> and APP<sup>wt</sup> littermate mice. As shown in Figure 2 (panels G, H and J), protein levels of Munc18-1 and synaptophysin in  $APP^{tg}p38\alpha^{fl/fl}Cre^{-/-}$  mice were significantly lower than levels of these proteins derived from  $APP^{wt}p38\alpha^{fl/fl}Cre^{+/-}$  and  $APP^{wt}p38\alpha^{fl/fl}Cre^{-/-}$  littermate mice (one-way ANOVA followed by post hoc test,  $P < .05$ ). Interestingly, the reduction in Munc18-1 and synaptophysin proteins due to APP-transgenic expression was rescued by the deletion of p38 $\alpha$ -MAPK in neurons (one-way ANOVA followed by *post-hoc* test,  $P < .05$ ). SNAP-25 protein levels were significantly higher in brains from  $APP^{tg}p38\alpha^{fl/fl}Cre^{+/-}$  mice than in brains from  $APP^{tg}p38\alpha^{fl/fl}Cre^{-/-}$  control mice (Figure 2G,I; one-way ANOVA followed by post hoc test,  $P < .05$ ). Comparison of  $APP^{wt}p38\alpha^{fl/fl}Cre^{+/-}$  and  $APP^{wt}p38\alpha^{fl/fl}Cre^{-/-}$  littermate mice showed no significant differences in protein levels of these four tested synaptic proteins (Figure 2G-K; one-way ANOVA followed by post hoc test,  $P > .05$ ).

To further clarify whether deletion of neuronal p38 $\alpha$ -MAPK protected synaptic integrity in APP<sup>tg</sup> mice, we evaluated the spine density and analyzed the morphology of spines of neurons in dendritic branches of apical dendrites in hippocampal CA1 and CA3 areas, and in the cortex layer II/III. Consistent with the Western blot results, Golgi staining revealed that the spine density of neurons in all three tested brain regions was significantly higher in  $APP^{tg}p38\alpha^{fl/fl}Cre^{+/-}$  mice than in

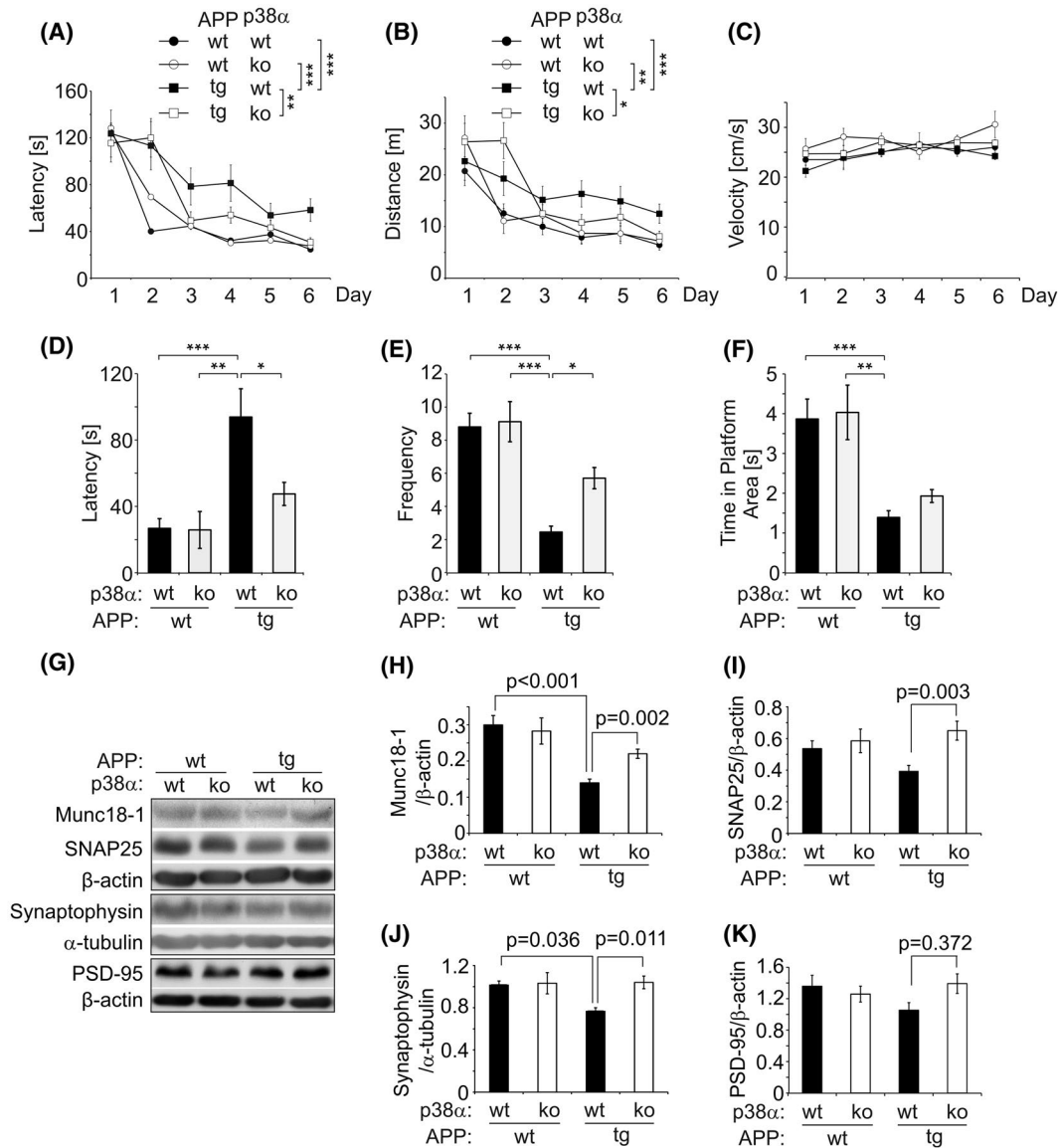


**FIGURE 2** Deletion of p38 $\alpha$ -MAPK in neurons improves cognitive function and attenuates synaptic impairments in APP-transgenic mice. During the training phase of the water maze test, 9-month-old APP-transgenic (tg) mice spent more time and traveled longer distances to reach the escape platform than did their non-APP-transgenic (APP<sup>wt</sup>) littermates. Deletion of p38 $\alpha$ -MAPK in neurons (p38 $\alpha$  ko) significantly reduced the traveling time and distance of APP<sup>tg</sup>, but not of APP<sup>wt</sup> mice after 3 days of training (A, B; two-way ANOVA from day 3 to day 6 followed by Bonferroni post hoc test, \*  $P < .05$ , \*\*  $P < .01$ , \*\*\*  $P < .001$ ;  $n \geq 13$  per group). However, deficiency of neuronal p38 $\alpha$ -MAPK affected the swimming speed neither of APP<sup>tg</sup> and APP<sup>wt</sup> mice, nor for each mouse at different training time points (C; two-way ANOVA,  $P > .05$ ;  $n \geq 13$  per group). In the probe trial, APP<sup>tg</sup> mice spent significantly longer in the first visit to the region where the platform was previously located, crossed the platform region with significantly less frequency and spent significantly less time in the platform region during the total 5-min experiment than APP<sup>wt</sup> mice; deletion of p38 $\alpha$ -MAPK in neurons partially recovered these APP expression-induced cognitive impairments (D-F; one-way ANOVA followed by Bonferroni post hoc test, \*  $P < .05$ , \*\*  $P < .01$ , \*\*\*  $P < .001$ ;  $n \geq 13$  per group). Western blotting was used to detect the amount of synaptic structure proteins, Munc18-1, SNAP25, synaptophysin, and PSD-95 in the brain homogenate of 9-month-old APP<sup>tg</sup> and APP<sup>wt</sup> mice (G-K). Deficiency in neuronal p38 $\alpha$ -MAPK was associated with higher levels of Munc18-1, SNAP25, and synaptophysin in the APP<sup>tg</sup> mouse, but not in the APP<sup>wt</sup> mouse (*t* test;  $n \geq 11$  per group)

APP<sup>tg</sup>p38 $\alpha$ <sup>fl/fl</sup>Cre<sup>-/-</sup> littermates (Figure S1A,B; *t* test,  $P < .05$ ). Moreover, dendritic spines were grouped into mature, immature and filopodia-like spines based on their morphologies.<sup>29</sup> Deficiency of p38 $\alpha$ -MAPK appeared to preserve more mature (mushroom-shaped) spines than the spines of other types of morphology (Figure S1C-G; *t* test,  $P < .05$ ).

### 3.3 | Deletion of neuronal p38 $\alpha$ -MAPK reduces cerebral A $\beta$ burden and neuroinflammation in APP-transgenic mice

After observing that deletion of p38 $\alpha$ -MAPK improved the cognitive performance in APP<sup>tg</sup> mice but not in APP<sup>wt</sup>

littermates, we analyzed A $\beta$  pathology in the AD mice, as A $\beta$  is the key molecule leading to neurodegeneration in AD.<sup>2</sup> We used the stereological *Cavalieri* method to measure A $\beta$  volume, adjusted relative to the volume of analyzed tissues, in 9-month-old APP<sup>tg</sup>p38 $\alpha^{fl/fl}$ Cre<sup>-/-</sup> and APP<sup>tg</sup>p38 $\alpha^{fl/fl}$ Cre<sup>+/-</sup> mice. The volume of immunoreactive A $\beta$  load in the APP<sup>tg</sup>p38 $\alpha^{fl/fl}$ Cre<sup>-/-</sup> mice (1.364%  $\pm$  0.140% in the hippocampus and 1.344%  $\pm$  0.096% in the cortex) was significantly higher than in the APP<sup>tg</sup>p38 $\alpha^{fl/fl}$ Cre<sup>+/-</sup> mice (0.876%  $\pm$  0.086% in the hippocampus and 0.847%  $\pm$  0.079%

in the cortex; Figure 3A,B; *t* test, *P* = .008 and 0.001, respectively), suggesting that deletion of p38 $\alpha$ -MAPK in neurons reduces the cerebral A $\beta$  burden.

Western blot analysis using human A $\beta$ -specific antibody was performed to determine the levels of A $\beta$  monomer, dimers and trimers and of C99 in the homogenate of cortex and hippocampus derived from 9-month-old APP<sup>tg</sup>p38 $\alpha^{fl/fl}$ Cre<sup>+/-</sup> and APP<sup>tg</sup>p38 $\alpha^{fl/fl}$ Cre<sup>-/-</sup> littermate mice. As shown in Figure 3C-E, deletion of p38 $\alpha$ -MAPK in neurons reduced all four detected peptides by 35% when

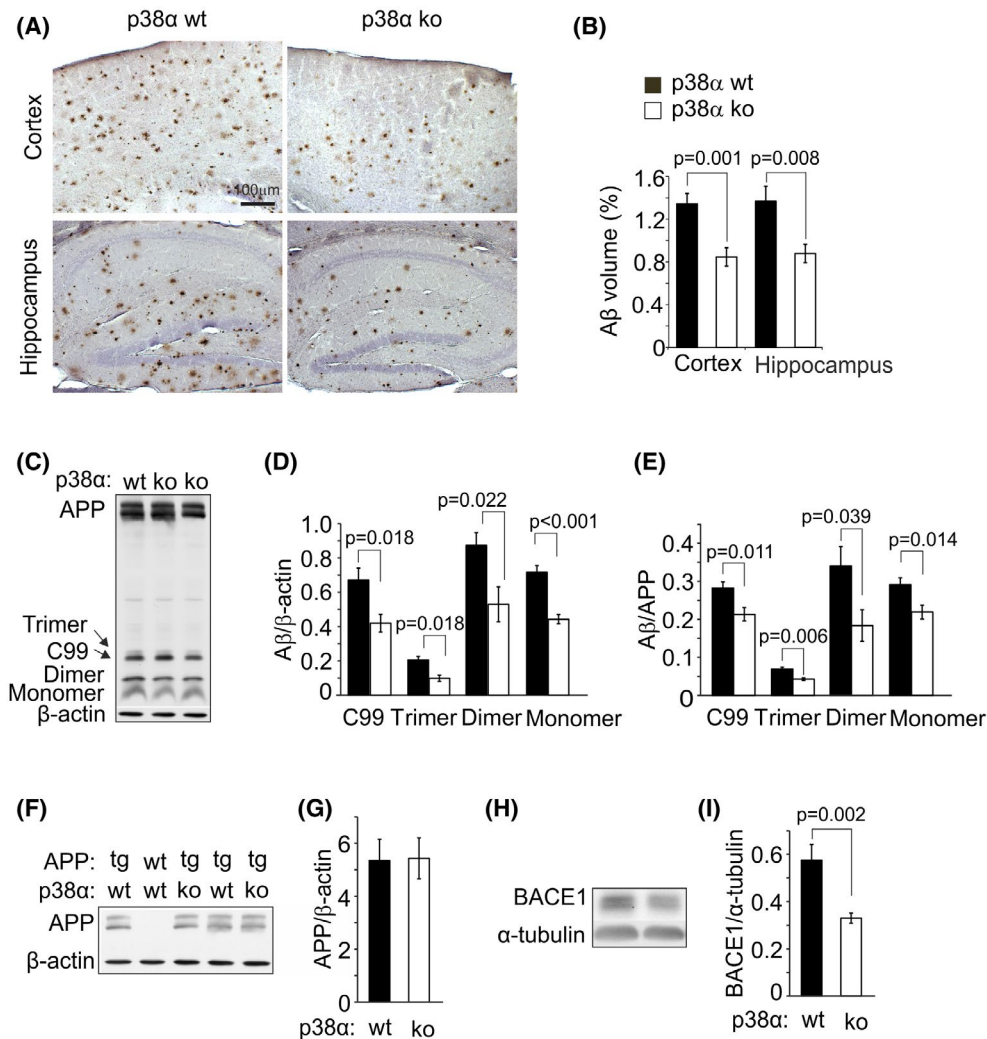


**FIGURE 3** Deletion of p38 $\alpha$ -MAPK in neurons reduces cerebral A $\beta$  in APP-transgenic mice. Nine-month-old APP-transgenic (tg) littermate mice with (ko) and without (wt) deletion of neuronal p38 $\alpha$ -MAPK were analyzed for cerebral A $\beta$  load after immunohistochemical staining of human A $\beta$  (A). The A $\beta$  volume was estimated with *Cavalieri* method and adjusted by the relevant brain volume. Deletion of p38 $\alpha$ -MAPK in neurons significantly reduced the cerebral A $\beta$  volume (B; *t* test; *n*  $\geq$  10 per group). The cerebral A $\beta$  in APP<sup>tg</sup> mice was also evaluated by detecting A $\beta$  in the brain homogenate with quantitative Western blot (C). Both, normalization of A $\beta$  against  $\beta$ -actin (D) and against APP (E), show reduced A $\beta$  load after deletion of p38 $\alpha$ -MAPK in neurons (C-E; *t* test; *n*  $\geq$  4 per group). The protein levels of APP were evaluated by quantitative Western blot and not different between APP<sup>tg</sup> mice with and without deletion of p38 $\alpha$ -MAPK (F and G; *t* test; *n*  $\geq$  8 per group). Deletion of p38 $\alpha$ -MAPK in neurons significantly reduced BACE1 protein in the brain of 9-month-old APP<sup>tg</sup> mice (H and I; *t* test; *n*  $\geq$  5 per group)

measured with  $\beta$ -actin as an internal control, or by 25% with APP as an internal control ( $t$  test,  $P < .05$ ). Moreover, we observed that APP proteins did not differ between APP<sup>tg</sup>p38 $\alpha$ <sup>fl/fl</sup>Cre<sup>+/-</sup> and APP<sup>tg</sup>p38 $\alpha$ <sup>fl/fl</sup>Cre<sup>-/-</sup> mice (F and G;  $t$  test,  $P > .05$ ); and BACE1 protein was significantly reduced in APP<sup>tg</sup>p38 $\alpha$ <sup>fl/fl</sup>Cre<sup>+/-</sup> mice (Figure 3H,I;  $t$  test  $P = .002$ ). Thus, the marked reduction of C99 fragments and A $\beta$  oligomers in the brain corroborated our recent findings that p38 $\alpha$ -MAPK deficiency inhibits the protein level and the activity of BACE1 in neurons and decreases cerebral A $\beta$  load.<sup>13</sup>

Microglial inflammatory activation as another important pathogenic mechanism in AD<sup>3</sup> had been analyzed with our established protocols.<sup>30</sup> We observed that deletion of p38 $\alpha$ -MAPK significantly reduced the number of Iba1-positive cells (Figure S2A,B;  $t$  test,  $P < .05$ ), downregulated the transcription of pro-inflammatory genes (*tnf- $\alpha$* , *il-1 $\beta$* , and *inos*) and upregulated transcription of anti-inflammatory genes (*il-10* and *mrc1*) in the brain of APP<sup>tg</sup> mice but not in APP<sup>wt</sup> mice (Figure S2C-J; one-way ANOVA followed by post hoc test,  $P < .05$ ). Deletion of neuronal p38 $\alpha$ -MAPK in APP<sup>tg</sup> mice also led to significantly upregulated transcription of *bdnf* and *igf-1* in the brain, both of which encode inflammation-related growth factors and promote neuronal protection and regeneration (Figure S2K,L; one-way ANOVA followed by post hoc test,  $P < .05$ ). The transcription of other tested genes, including *ccl-2*, *arg1*, and *chi3l3*, in APP<sup>tg</sup> mouse brains was not changed by neuronal deficiency of p38 $\alpha$ -MAPK (Figure S2E,H,J; one-way ANOVA followed by post hoc test,  $P > .05$ ).

### 3.4 | Deletion of neuronal p38 $\alpha$ -MAPK alters gene expression profile in APP-transgenic mice

After observing that deletion of neuronal p38 $\alpha$ -MAPK improved cognitive function in APP<sup>tg</sup> mice, we performed transcriptome analysis to identify potential mechanisms that mediate neuronal protection. Next-generation sequencing of mRNA isolated from cortex and hippocampus of APP<sup>tg</sup>p38 $\alpha$ <sup>fl/fl</sup>Cre<sup>+/-</sup> and APP<sup>tg</sup>p38 $\alpha$ <sup>fl/fl</sup>Cre<sup>-/-</sup> littermate mice resulted in 36 437 sequenced transcript identifications for 15 011 individual genes with different transcript variants. Among identified gene transcripts, 253 gene transcripts were altered by log<sub>2</sub> fold change  $< -2$  or  $> 2$  and with a FDR corrected  $P < .01$ . From these altered gene transcripts 107 were downregulated and 146 were upregulated in APP<sup>tg</sup>p38 $\alpha$ <sup>fl/fl</sup>Cre<sup>+/-</sup> mice as compared with APP<sup>tg</sup>p38 $\alpha$ <sup>fl/fl</sup>Cre<sup>-/-</sup> littermate controls (see Figure 4A,B). All significantly altered transcripts, also with  $P$  value of  $< .05$ , are shown by their gene name and with their corresponding log FC and FDR values in Table S1.

By applying the Kyoto Encyclopedia of Genes and Genomes pathway analysis tool of the Pathview annotation software, we performed pathway enrichment analysis of all 253 significantly altered gene transcripts. Pathways such as MAPK signaling, spliceosome formation and calcium signaling were found to be enriched for genes differentially regulated by neuronal deletion of p38 $\alpha$ -MAPK. Heat maps showed the differences in transcript variants of gene expression (Figure 4C-E). As expected, the MAPK signaling pathway was altered in p38 $\alpha$ -MAPK-deficient mouse brain. In this pathway, the gene transcription of *mapk9*, also known as C-Jun N-terminal kinase (*jnk2*) was strongly upregulated in p38 $\alpha$ -MAPK-deficient mouse brain, which might indicate a compensatory mechanism. JNK2 acts in a parallel MAPK signaling cascade and shares some common substrates with p38 $\alpha$ -MAPK. Interestingly, the transcription of genes associated with the spliceosome was significantly modified by deletion of neuronal p38 $\alpha$ -MAPK, which might represent an important mechanism through which p38 $\alpha$ -MAPK regulates gene transcription, as the spliceosome removes introns from a transcribed precursor messenger RNA (pre-mRNA).<sup>41</sup> Indeed disturbance in spliceosome function with reduced maturation of pre-mRNA has been reported in A $\beta$ -challenged neuronal cells.<sup>42</sup> In addition to these genes that were included into the enrichment analysis (see Figure 4E), there were 11 calcium signaling-related genes (*adarb1*, *ano4*, *dtnb*, *map2*, *nfatc2*, *plch1*, *s100a5*, *sox5*, *tec*, *tfap2b*, and *tmem63c*), whose transcription was also significantly changed by deletion of p38 $\alpha$ -MAPK in neurons (see Table S1). Using the online database, Panglaodb (<https://panglaodb.se/>), we analyzed the cellular origin of transcriptionally altered genes. We observed that these spliceosome pathway and calcium signaling-related genes whose transcription was changed by p38 $\alpha$ -MAPK deficiency were enriched in neuronal populations instead of in microglia and other glial cells.<sup>43</sup>

To validate the results derived from sequencing experiments, we performed quantitative RT-PCR to measure transcripts of the following genes, which are involved in calcium signaling and/or synaptic plasticity: *adc3*, *adc7*, *atp2b4*, *gnas*, *grin2a*, *htr7*, *slc8a1*, *sphk1*, *tmem63c*, *plch1*, and *nfatc2*. As shown in Figure 5, the alteration of gene transcription screened by next-generation sequencing could be confirmed by PCR ( $t$  test,  $P < .05$ ).

### 3.5 | Deletion of neuronal p38 $\alpha$ -MAPK differently regulates glutamate and NMDA-induced calcium influx and cell death in primary cultured neurons

After observing that p38 $\alpha$ -MAPK deficiency altered the transcription of calcium homeostasis-related genes in brain tissues, we asked whether p38 $\alpha$ -MAPK regulates

the calcium influx in neurons. We cultured p38 $\alpha$ -deficient and wild-type cortical neurons from the breeding between APP<sup>tg</sup>p38<sup>fl/fl</sup>Nex-Cre<sup>+/-</sup> (or APP<sup>wt</sup>p38<sup>fl/fl</sup>Nex-Cre<sup>+/-</sup>)

male mice and APP<sup>wt</sup>p38<sup>fl/fl</sup>Nex-Cre<sup>-/-</sup> female mice. We first validated the neuronal reduction of p38 $\alpha$ -MAPK by quantitative Western blot. The p38 $\alpha$ -MAPK-deficient

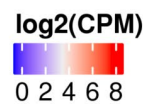
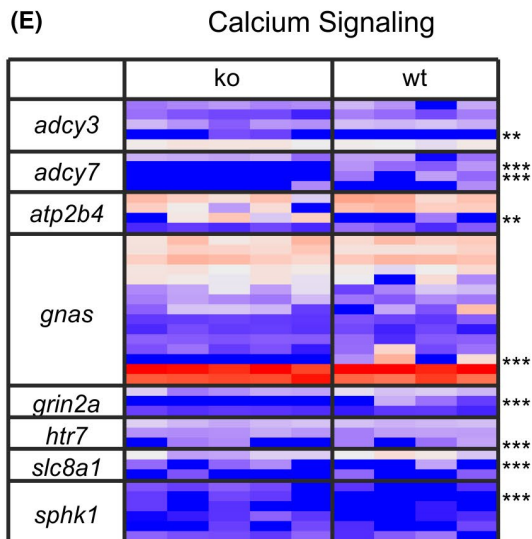
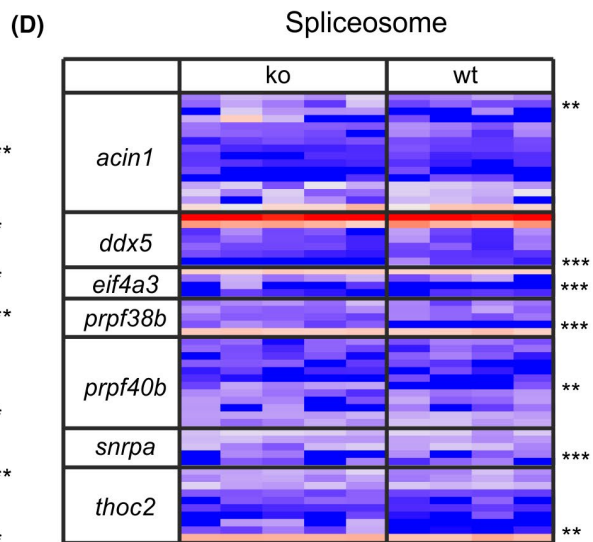
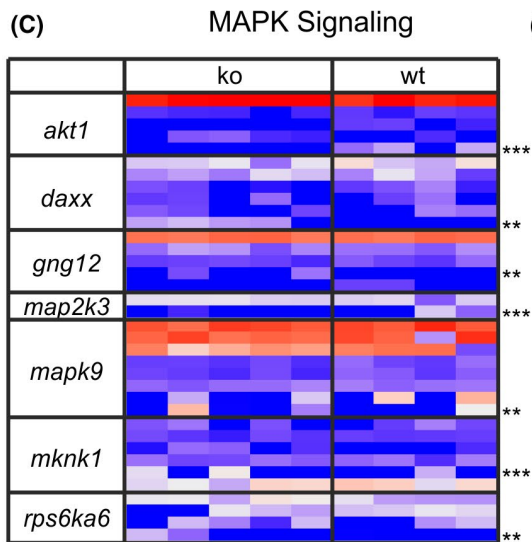
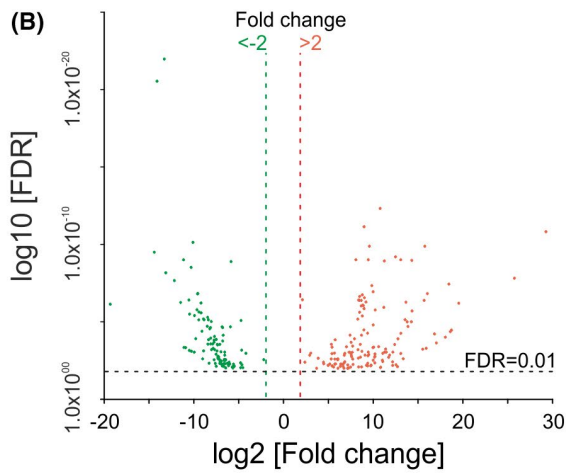
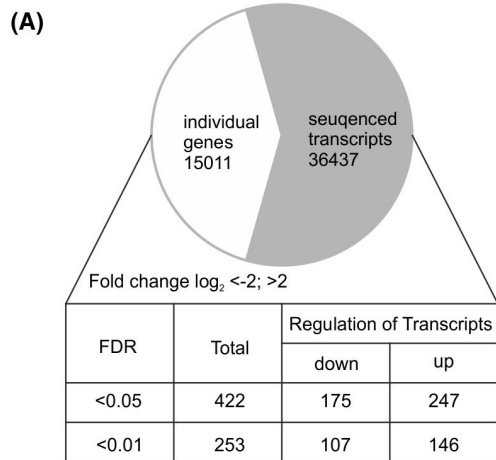


**FIGURE 4** Deletion of p38 $\alpha$ -MAPK in neurons changes cerebral gene expression in APP-transgenic mice. A, Next generation sequencing of mRNA libraries prepared from 9-month-old neuronal p38 $\alpha$ -MAPK-deficient (ko; n = 5) and wild-type (wt; n = 4) APP-transgenic mouse brains identified 36 437 transcripts and 15 011 individual genes. Among these gene transcripts, 253 were altered (107 downregulated and 140 upregulated) by p38 $\alpha$ -MAPK deficiency with log<sub>2</sub>-folded changes <-2 or >2 and corrected *P* values of FDR < 0.01. B, Volcano plot shows the fold changes of gene transcripts (log<sub>2</sub> scale) in p38 $\alpha$ -MAPK ko mouse brain compared to wt mouse brains (x-axis) and relevant significance (y-axis, log<sub>10</sub> scale). Downregulation is marked in green and upregulation in red. C-E, Heat maps reveal differently expressed transcript variants of genes. Each gene has different transcript variants, the significantly altered ones are indicated with the star of significance. Data are expressed as mean fragments per kilobase of transcript per million reads (FPKM), standardized, and visualized using the MATLAB clustergram script. Red, relatively high expression; blue, relatively low expression in p38 $\alpha$ -MAPK ko mice; \*\* for FDR < 0.01 and \*\*\* for FDR < 0.001

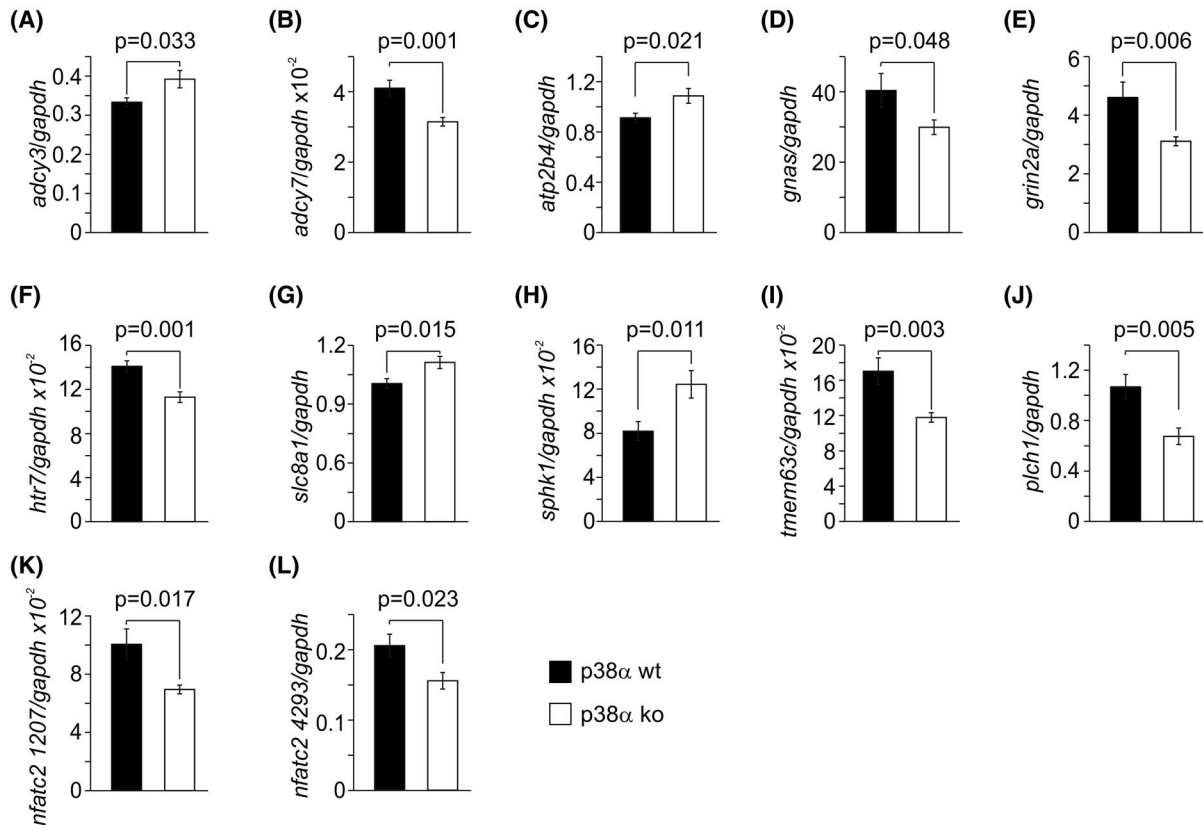


**FIGURE 5** Deletion of p38 $\alpha$ -MAPK alters transcription of calcium signaling and synaptic plasticity-related genes in APP-transgenic mouse brain. Nine-month-old APP-transgenic mice with (ko) and without (wt) deletion of neuronal p38 $\alpha$ -MAPK were analyzed for transcriptions of calcium signaling and synaptic plasticity-related genes. Total RNA was isolated from the brain and reverse transcribed. Real-time PCR was used to detect gene transcripts (*t* test; n  $\geq$  7 per group)

neurons (APP<sup>tg</sup>p38<sup>fl/fl</sup>Nex-Cre<sup>+/-</sup>) showed a reduced protein level of p38-MAPK by nearly 80% compared to the wild-type neurons (APP<sup>tg</sup>p38<sup>fl/fl</sup>Nex-Cre<sup>-/-</sup>) (Figure 6A; *t* test, *P* = .026). Interestingly, we observed that the protein level of Grin2a, a subunit of NMDAR, was lower in p38 $\alpha$ -MAPK-deficient neurons than in wild-type cells (Figure 6B; *t* test, *P* = .010).

Then, we examined effects of APP/PS1-overexpression on calcium influx. We challenged APP<sup>tg</sup>p38<sup>fl/fl</sup>Nex-Cre<sup>-/-</sup> and APP<sup>wt</sup>p38<sup>fl/fl</sup>Nex-Cre<sup>-/-</sup> neurons with L-glutamate (at 100 and 500  $\mu$ M) or NMDA (at 50  $\mu$ M and 10mM) followed by 75 mM KCl. The calcium influx was not different between these two groups of neurons (Figure S3A,B; n  $\geq$  3 animals

per group). In the culture medium of APP/PS1-transgenic neurons, we could not detect A $\beta$  with Western blot (data not shown). The concentration of A $\beta$  in calcium imaging chamber should be even lower after cells were further perfused with A $\beta$ -free imaging buffer. We supposed that A $\beta$  at such a low level was not able to trigger calcium influx as previously reported.<sup>44</sup> Moreover, overexpression of PS1 appeared not to alter glutamate receptors-mediated calcium influx in our cultured neurons, although mutant PS1 potentially regulates calcium release from endoplasmic reticulum and affect store-operated calcium channels.<sup>45</sup> Thus, we used both APP-transgenic (APP<sup>tg</sup>) and wild-type (APP<sup>wt</sup>) neurons for the following experiments.

We treated  $APP^{wt}p38^{fl/fl}Nex-Cre^{+/-}$  and  $APP^{wt}p38^{fl/fl}Nex-Cre^{-/-}$  neurons with 75 mM KCl to induce membrane depolarization. Substantial calcium influx was clearly

induced in both neurons and the responses were higher in  $p38\alpha$ -MAPK-deficient neurons than in  $p38\alpha$ -MAPK-wild-type cells (Figure 6C; two-way ANOVA,  $P < .001$ ). When

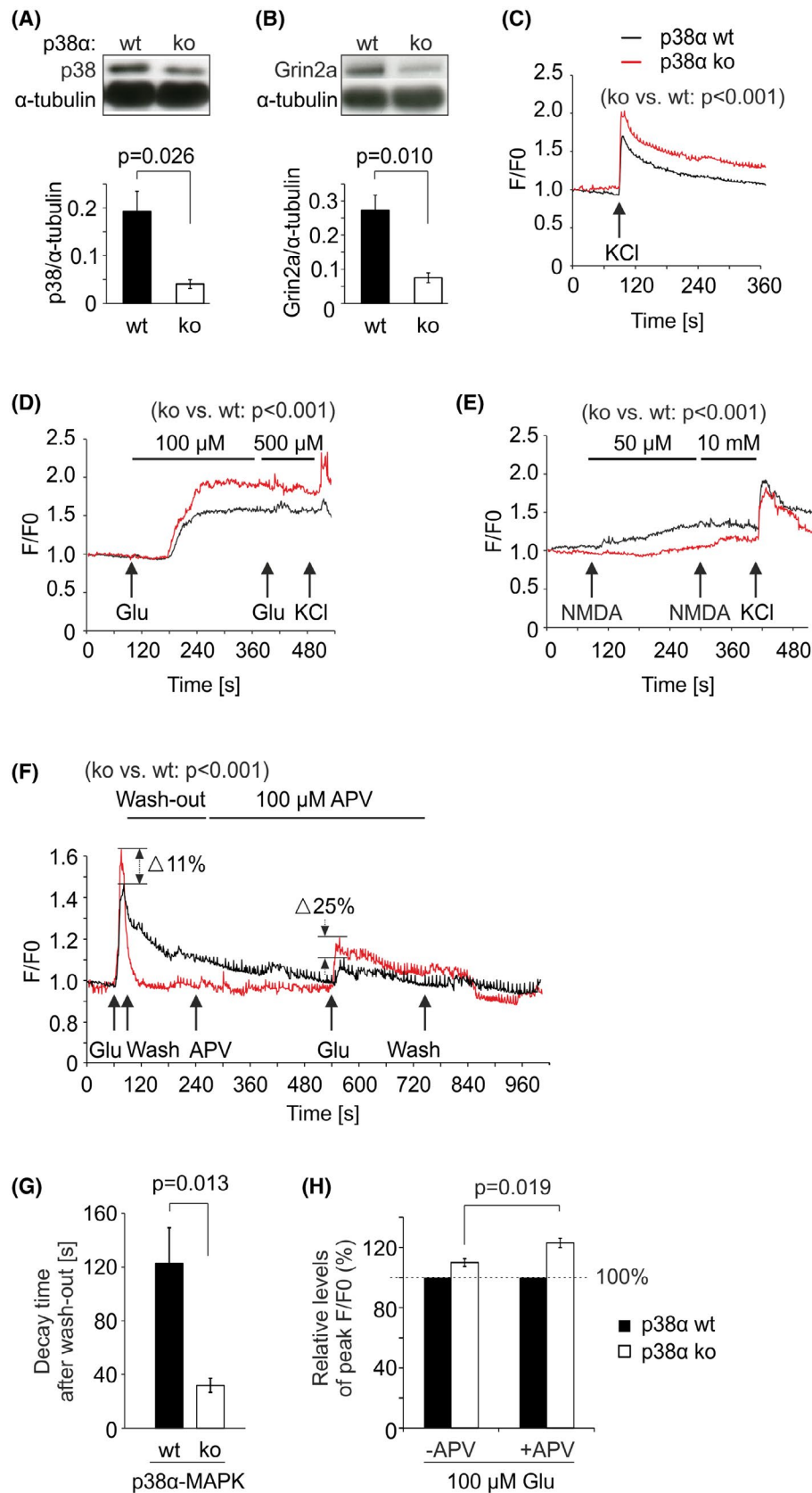


**FIGURE 6** Deletion of p38 $\alpha$ -MAPK reduces Grin2a proteins and regulates calcium influx in primary neurons. Primary neurons were cultured from neuronal p38 $\alpha$ -MAPK deficient (ko) and wild-type (wt) embryos. Western blot detected lower protein levels of p38-MAPK and NMDAR subunit Grin2a (A and B; *t* test,  $n \geq 5$  per group). Fluo-4 fluorescent intensity (F) in neurons was measured before and after stimulation with: i) 75 mM KCl alone (C), ii) 100  $\mu$ M, 500  $\mu$ M L-glutamate (Glu) and 75 mM KCl (D), and iii) 50  $\mu$ M, 10 mM NMDA and 75 mM KCl (E). *F*<sub>0</sub> was recorded at 0 second. Deletion of p38 $\alpha$ -MAPK enhanced KCl or Glu-triggered but inhibited NMDA-initiated calcium influx (C-E; two-way ANOVA showing difference between p38 $\alpha$ -MAPK ko and wt cells;  $n \geq 7$  per group. For each group, more than 481 neurons were analyzed). As shown in (F), p38 $\alpha$ -MAPK-ko and wt neurons were also serially treated with: i) 100  $\mu$ M L-Glu for 20 s, ii) washing out for 160 s, iii) 100  $\mu$ M NMDAR antagonist, APV-2, for 300 s, and iv) 100  $\mu$ M L-Glu together with APV-2 for 20 s. During wash-out phase, the intensity of Fluo-4 fluorescence dropped down much faster in p38 $\alpha$ -MAPK-ko cells than in wt neurons (two-way ANOVA showing effects of genotypes;  $n \geq 4$  per group, in which total 26 ko neurons and 112 wt neurons were analyzed). The decay time for the Fluo-4 fluorescence was significantly shorter in p38 $\alpha$ -MAPK-ko cells than in wt neurons (G; *t* test,  $n \geq 4$  per group). The increase ( $\Delta$ ) of Glu-induced peak *F*/*F*<sub>0</sub> in p38 $\alpha$ -MAPK-ko neurons compared with that in p38 $\alpha$ -MAPK-wt neurons (set at 100%) was calculated. Interestingly,  $\Delta$ (*F*/*F*<sub>0</sub>) was significantly higher during Glu treatment in the presence of APV-2 than during the treatment with Glu alone (H; *t* test,  $n \geq 4$  per group)

cells were activated with 100  $\mu$ M and 500  $\mu$ M L-glutamate, deletion of p38 $\alpha$ -MAPK significantly enhanced calcium influx as compared with p38 $\alpha$ -MAPK-wild-type cells (Figure 6D; two-way ANOVA,  $P < .001$ ). The calcium influx could be further induced by adding 75 mM KCl after glutamate treatments. Similarly, we treated neurons with NMDAR-specific agonist, NMDA. Interestingly, p38 $\alpha$ -MAPK-deficient neurons showed little calcium influx (*F*/*F*<sub>0</sub> from 0.990 to 1.159) even after application of 10 mM NMDA, whereas, p38 $\alpha$ -MAPK-wild-type neurons demonstrated pronounced calcium influx after treatment with 50  $\mu$ M NMDA (*F*/*F*<sub>0</sub> from 1.00 to 1.286) (Figure 6E; two-way ANOVA,  $P < .001$ ). After NMDA treatments, p38 $\alpha$ -MAPK-deficient and wild-type cells were further stimulated with 75 mM KCl and displayed a comparable increase of calcium signals, which indicated that the mild elevation of calcium signal in p38 $\alpha$ -MAPK-deficient neurons was not due to the neurotoxicity of NMDA.

We also treated APP<sup>tg</sup>p38<sup>fl/fl</sup>Nex-Cre<sup>+/-</sup> and APP<sup>tg</sup>p38<sup>fl/fl</sup>Nex-Cre<sup>-/-</sup> neurons with 100  $\mu$ M L-glutamate. The peak level of calcium influx in p38 $\alpha$ -MAPK-deficient neurons was significantly higher than in p38 $\alpha$ -MAPK-wild-type neurons (Figure 6F; *F*/*F*<sub>0</sub>:  $1.67 \pm 0.04$  vs  $1.52 \pm 0.04$  in APP<sup>tg</sup>p38<sup>fl/fl</sup>Nex-Cre<sup>+/-</sup> and APP<sup>tg</sup>p38<sup>fl/fl</sup>Nex-Cre<sup>-/-</sup> neurons, respectively; *t* test,  $P = .037$ ). Interestingly, when L-glutamate was washed out, the intensity of calcium-associated Fluo-4 fluorescence dropped significantly faster in p38 $\alpha$ -MAPK-deficient neurons than in p38 $\alpha$ -MAPK-wild-type neurons (Figure 6F; two-way ANOVA,  $P < .001$ ). The decay time for calcium fluorescence was  $32.00 \pm 5.34$  seconds vs  $123.00 \pm 26.47$  seconds in APP<sup>tg</sup>p38<sup>fl/fl</sup>Nex-Cre<sup>+/-</sup> and APP<sup>tg</sup>p38<sup>fl/fl</sup>Nex-Cre<sup>-/-</sup> neurons, respectively (Figure 6G; *t* test,  $P = .013$ ).

To investigate how p38 $\alpha$ -MAPK deficiency enhanced calcium influx, we continued to co-treat APP<sup>tg</sup>p38<sup>fl/fl</sup>Nex-Cre<sup>+/-</sup> and APP<sup>tg</sup>p38<sup>fl/fl</sup>Nex-Cre<sup>-/-</sup> neurons from the wash-out experiment with 100  $\mu$ M L-glutamate and a NMDAR antagonist, APV-2. Calcium flux was again induced although the intra-neuronal levels of calcium were lower than in cells treated with glutamate alone (Figure 6F). The peak level of calcium influx in p38 $\alpha$ -MAPK-deficient

neurons was still higher than that in p38 $\alpha$ -MAPK-wild-type neurons (Figure 6F; *F*/*F*<sub>0</sub>:  $1.34 \pm 0.03$  vs  $1.09 \pm 0.03$  in APP<sup>tg</sup>p38<sup>fl/fl</sup>Nex-Cre<sup>+/-</sup> and APP<sup>tg</sup>p38<sup>fl/fl</sup>Nex-Cre<sup>-/-</sup> cells, respectively; *t* test,  $P = .001$ ). When p38 $\alpha$ -MAPK deficiency-associated enhancement of calcium influx was compared in neurons that were challenged with L-glutamate in presence and absence of APV-2, we observed that blocking NMDAR potentially amplified the effect of p38 $\alpha$ -MAPK deficiency on calcium influx. When peak levels of calcium influx in p38 $\alpha$ -MAPK-wild-type neurons were set at 100% in both experimental settings, p38 $\alpha$ -MAPK deletion elevated maximal calcium influx to  $122.93 \pm 3.11\%$  in the presence of APV-2 and to  $109.99 \pm 2.61\%$  in the absence of APV-2 (Figure 6F,H; *t* test,  $P = .019$ ).

In the end, we analyzed the neurotoxic effects of calcium influx upon challenges of L-glutamate and NMDA. Deletion of p38 $\alpha$ -MAPK significantly inhibited activation of caspase-3 in cultured neurons after treatments with both L-glutamate at 100  $\mu$ M (Figure 7A) and NMDA at 50  $\mu$ M (Figure 7B) (*t* test between p38 $\alpha$ -MAPK deficient and wild-type neurons,  $P = .032$  for L-glutamate and 0.039 for NMDA).

### 3.6 | Deletion of p38 $\alpha$ -MAPK in neurons attenuates cognitive deficits and synaptic impairments in Tau-transgenic mice

APP<sup>tg</sup> mice cannot model all pathological changes of AD, such as those associated with p-Tau. To investigate the effects of neuronal p38 $\alpha$ -MAPK on the Tau-associated pathological changes in AD, we cross-bred p38 $\alpha$ <sup>fl/fl</sup> mice,<sup>25</sup> Nex-Cre mice,<sup>26</sup> and P301S Tau-transgenic (Tau<sup>tg</sup>) mice<sup>27</sup> to create neuronal p38 $\alpha$ -MAPK-deficient Tau<sup>tg</sup> AD mice. The lower level of p38-MAPK protein in the brain homogenate derived from Tau<sup>tg</sup>p38 $\alpha$ <sup>fl/fl</sup>Cre<sup>+/-</sup> mice compared to Tau<sup>tg</sup>p38 $\alpha$ <sup>fl/fl</sup>Cre<sup>-/-</sup> mice confirmed the deletion of p38 $\alpha$ -MAPK (Figure 8A; *t* test,  $P < .001$ ). We also measured p38-MAPK activities in brains of 9-month-old Tau<sup>tg</sup>p38 $\alpha$ <sup>fl/fl</sup>Cre<sup>+/-</sup> and Tau<sup>tg</sup>p38 $\alpha$ <sup>fl/fl</sup>Cre<sup>-/-</sup> mice,

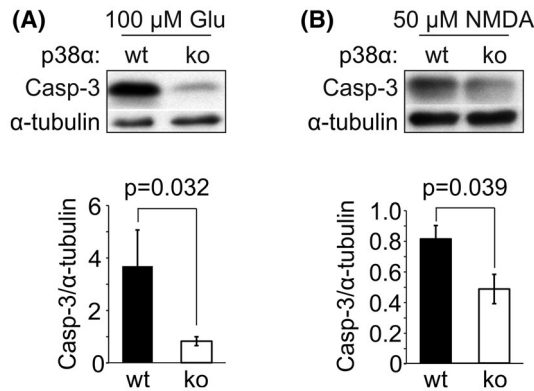


**FIGURE 7** Deletion of p38 $\alpha$ -MAPK attenuates both L-glutamate and NMDA-induced apoptosis in primary neurons. Primary neurons were cultured from APP-transgenic embryos with (ko) and without (wt) deletion of p38 $\alpha$ -MAPK in neurons. Western blot detected significant reduction of cleaved caspase-3 (Casp-3) in p38 $\alpha$ -MAPK-ko cells compared with p38 $\alpha$ -MAPK-wt controls after treatments with 100  $\mu$ M L-glutamate (Glu) (A; *t* test;  $n \geq 4$  per group) and 50  $\mu$ M NMDA (B; *t* test;  $n \geq 4$  per group) for 16 h

and their non-Tau-transgenic (Tau<sup>wt</sup>) littermate controls (Tau<sup>wt</sup>p38 $\alpha$ <sup>fl/fl</sup>Cre<sup>+/-</sup> and Tau<sup>wt</sup>p38 $\alpha$ <sup>fl/fl</sup>Cre<sup>-/-</sup>). The phosphorylation of p38-MAPK was increased in the brain of Tau<sup>tg</sup> mice compared to Tau<sup>wt</sup> mice. Deletion of p38 $\alpha$ -MAPK inhibited the phosphorylation of p38 $\alpha$ -MAPK in Tau<sup>tg</sup> mouse brain but not in Tau<sup>wt</sup> brain (Figure 8C,D; one-way ANOVA,  $P < .05$ ).

We have recently observed that the cognitive function of Tau<sup>tg</sup> mice is impaired in the Morris water maze test.<sup>28</sup> Compared to Tau<sup>tg</sup>p38 $\alpha$ <sup>fl/fl</sup>Cre<sup>-/-</sup> littermates, 9-month-old Tau<sup>tg</sup>p38 $\alpha$ <sup>fl/fl</sup>Cre<sup>+/-</sup> mice traveled in significantly less time and over less distance to reach the escaping platform in the training phase, but the swimming velocity did not differ between these two groups of mice (Figure 8E-G; two-way ANOVA,  $P < .05$ ). Similarly, in the probe trial, Tau<sup>tg</sup>p38 $\alpha$ <sup>fl/fl</sup>Cre<sup>+/-</sup> mice found the original region for platform within a shorter time, crossed the target position more frequently and explored in the target region for longer duration than Tau<sup>tg</sup>p38 $\alpha$ <sup>fl/fl</sup>Cre<sup>-/-</sup> littermates (Figure 8H-J; *t* test,  $P < .05$ ).

Levels of the synaptic structure proteins Munc18-1, PSD-95, and synaptophysin are reduced in the brains of Tau<sup>tg</sup> mice compared to wild-type (Tau<sup>wt</sup>) controls.<sup>28</sup> Interestingly, the protein levels of Munc18-1 and synaptophysin in brain homogenates of 9-month-old Tau<sup>tg</sup>p38 $\alpha$ <sup>fl/fl</sup>Cre<sup>+/-</sup> mice were significantly elevated by the deletion of p38 $\alpha$ -MAPK in neurons compared to Tau<sup>tg</sup>p38 $\alpha$ <sup>fl/fl</sup>Cre<sup>-/-</sup> mice (Figure 8K,M; *t* test,  $P < .05$ ). Deletion of neuronal p38 $\alpha$ -MAPK in Tau<sup>tg</sup> mice tended to restore the cerebral protein level of PSD-95, but the change was not significant (Figure 8N; *t* test,  $P = .05$ ).

### 3.7 | Deletion of p38 $\alpha$ -MAPK in neurons reduces cerebral p-Tau protein in Tau-transgenic mice

As p-Tau mediates toxic effects of A $\beta$  in AD pathogenesis,<sup>46,47</sup> we investigated effects of neuronal deficiency of p38 $\alpha$ -MAPK on cerebral p-Tau levels. We counted AT8-positive cells in cortex and hippocampus of 9-month-old Tau<sup>tg</sup>p38 $\alpha$ <sup>fl/fl</sup>Cre<sup>-/-</sup> and Tau<sup>tg</sup>p38 $\alpha$ <sup>fl/fl</sup>Cre<sup>+/-</sup> mice. The total number of AT8-immunoreactive cells adjusted to the investigated area in Tau<sup>tg</sup>p38 $\alpha$ <sup>fl/fl</sup>Cre<sup>-/-</sup> mice ( $16.51 \pm 1.94/\text{mm}^2$  in cortex and  $35.40 \pm 4.75/\text{mm}^2$  in hippocampus) was significantly higher than that in Tau<sup>tg</sup>p38 $\alpha$ <sup>fl/fl</sup>Cre<sup>+/-</sup> mice ( $7.50 \pm 2.53/\text{mm}^2$  in cortex, and  $18.71 \pm 4.34/\text{mm}^2$  in hippocampus; Figure 9A,B; *t* test for Tau<sup>tg</sup>p38 $\alpha$ <sup>fl/fl</sup>Cre<sup>+/-</sup> vs Tau<sup>tg</sup>p38 $\alpha$ <sup>fl/fl</sup>Cre<sup>-/-</sup> mice,  $P = .013$  and  $0.021$ , respectively). We also stained brain tissues with thioflavine S to identify neurofibrillary tangles using a published method.<sup>31</sup> We observed very few thioflavine staining-positive cells in the whole brain (Figure 9C). However, deletion of p38 $\alpha$ -MAPK did reduce the number of staining-positive cells in both cortex and hippocampus (Figure 9D; *t* test,  $P = .039$  and  $0.039$ , respectively).

We extracted Tau proteins from 9-month-old Tau<sup>tg</sup>p38 $\alpha$ <sup>fl/fl</sup>Cre<sup>+/-</sup> and Tau<sup>tg</sup>p38 $\alpha$ <sup>fl/fl</sup>Cre<sup>-/-</sup> mice with RAB, RIPA, and FA buffers. Western blots revealed that both the protein levels of p-Tau seen with direct densitometry and ratios of p-Tau/t-Tau were significantly lower in RIPA and FA fractions derived from Tau<sup>tg</sup>p38 $\alpha$ <sup>fl/fl</sup>Cre<sup>+/-</sup> mice, compared to Tau<sup>tg</sup>p38 $\alpha$ <sup>fl/fl</sup>Cre<sup>-/-</sup> mice (Figure 9F,G; *t* test,  $P < .05$ ). In the RAB fraction, deletion of neuronal p38 $\alpha$ -MAPK tended to decrease the cerebral p-Tau level in Tau<sup>tg</sup> mice, although the difference was not significant (Figure 9E; *t* test,  $P > .05$ ). In all three fractions of brain homogenate, Tau<sup>tg</sup>p38 $\alpha$ <sup>fl/fl</sup>Cre<sup>+/-</sup> and Tau<sup>tg</sup>p38 $\alpha$ <sup>fl/fl</sup>Cre<sup>-/-</sup> littermate mice did not differ in t-Tau protein levels (data not shown).

We have recently observed that activated autophagy is able to degrade p-Tau in the tau-transgenic mouse brain.<sup>28</sup> We further detected autophagy markers, LC3B-I and LC3B-II, in RIPA-soluble brain homogenate. As shown in Figure 9H, the ratio of LC3B-III/I was significantly higher in Tau<sup>tg</sup>p38 $\alpha$ <sup>fl/fl</sup>Cre<sup>+/-</sup> mouse brain than that in Tau<sup>tg</sup>p38 $\alpha$ <sup>fl/fl</sup>Cre<sup>-/-</sup> mice (*t* test,  $P < .05$ ).

## 4 | DISCUSSION

A $\beta$  and p-Tau are two major pathogenic molecules in AD. In our study, we demonstrated that deletion of neuronal p38 $\alpha$ -MAPK improves cognitive function of both 9-month-old APP and tau-transgenic AD mice, which is associated with reduced A $\beta$  and p-Tau load, and shifting from pro- to anti-inflammatory activation in the brain. We

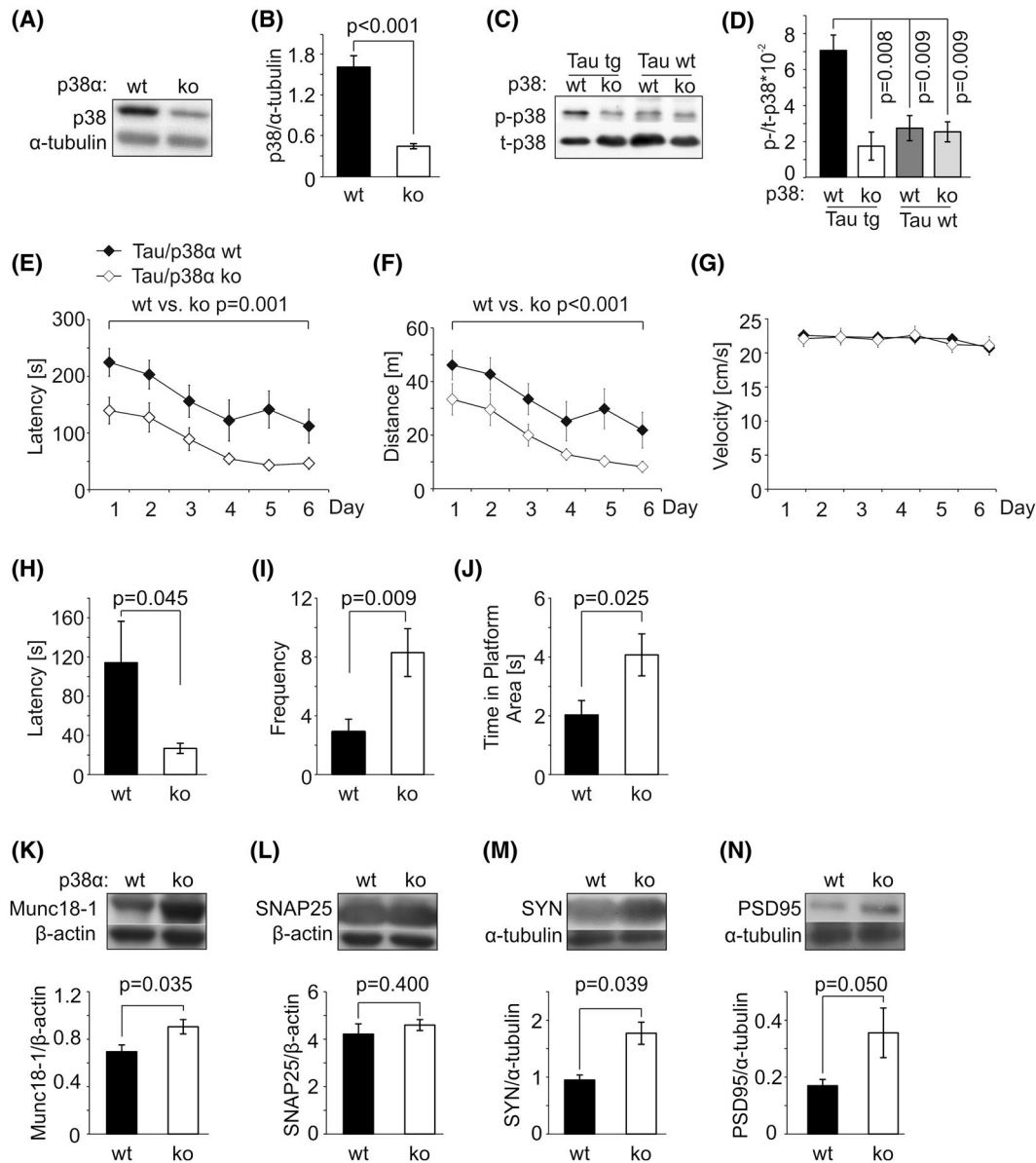


**FIGURE 8** Deletion of p38 $\alpha$ -MAPK in neurons improves cognitive function and attenuates synaptic impairments in Tau-transgenic mice. The deletion of p38 $\alpha$ -MAPK in Tau-transgenic (tg) mice was confirmed by detecting p38-MAPK in the brain homogenate with quantitative Western blot (A and B;  $t$  test;  $n \geq 8$  per group). The homogenates of brain derived from 9-month-old Tau<sup>tg</sup> and non-Tau-transgenic (wt) littermate mice with (ko) without (wt) deletion of p38 $\alpha$ -MAPK were analyzed for phosphorylated (p-p38) and total (t-p38) p38-MAPK with Western blot. In this experiment, the loading protein for each lane was adapted to have similar amount of t-p38. The protein level of p-p38 in Tau<sup>tg</sup> mice with normal expression of p38 $\alpha$ -MAPK was higher than in Tau<sup>wt</sup> littermates. Deletion of p38 $\alpha$ -MAPK reduced phosphorylation of p38-MAPK in Tau<sup>tg</sup> mice but not in Tau<sup>wt</sup> mice (C and D, one-way ANOVA followed by Bonferroni post hoc test,  $n \geq 4$  per group). Morris water maze was performed to evaluate the cognitive function of 9-month-old Tau<sup>tg</sup> mice with and without deletion of p38 $\alpha$ -MAPK in neurons. During the training phase, p38 $\alpha$ -MAPK wt mice spent significantly more time and traveled longer distances to reach the hidden platform than did their p38 $\alpha$ -MAPK ko littermates. The swimming speed was not different between both genotypes (E-G; two-way ANOVA showing the effect of genotype;  $n \geq 8$  per group). In the probe trial, Tau<sup>tg</sup> p38 $\alpha$ -MAPK ko mice spent significantly shorter time in the first visit of the region where the platform was previously located, crossed the platform region with significantly more frequency and spent significantly longer time in the platform region during the total 5-minute experiment than their Tau<sup>tg</sup> p38 $\alpha$ -MAPK wt littermates (H-J;  $t$  test;  $n \geq 8$  per group). After water maze, the brain was collected for further biochemical analysis. The amount of synaptic structure proteins, such as Munc18-1, SNAP25, synaptophysin (SYN), and PSD95, was quantified with Western blot (K-N). Neuronal deficiency of p38 $\alpha$ -MAPK was associated with a higher level of Munc18-1, synaptophysin and PSD95 in Tau<sup>tg</sup> mice (K, M and N;  $t$  test;  $n \geq 5$  per group)

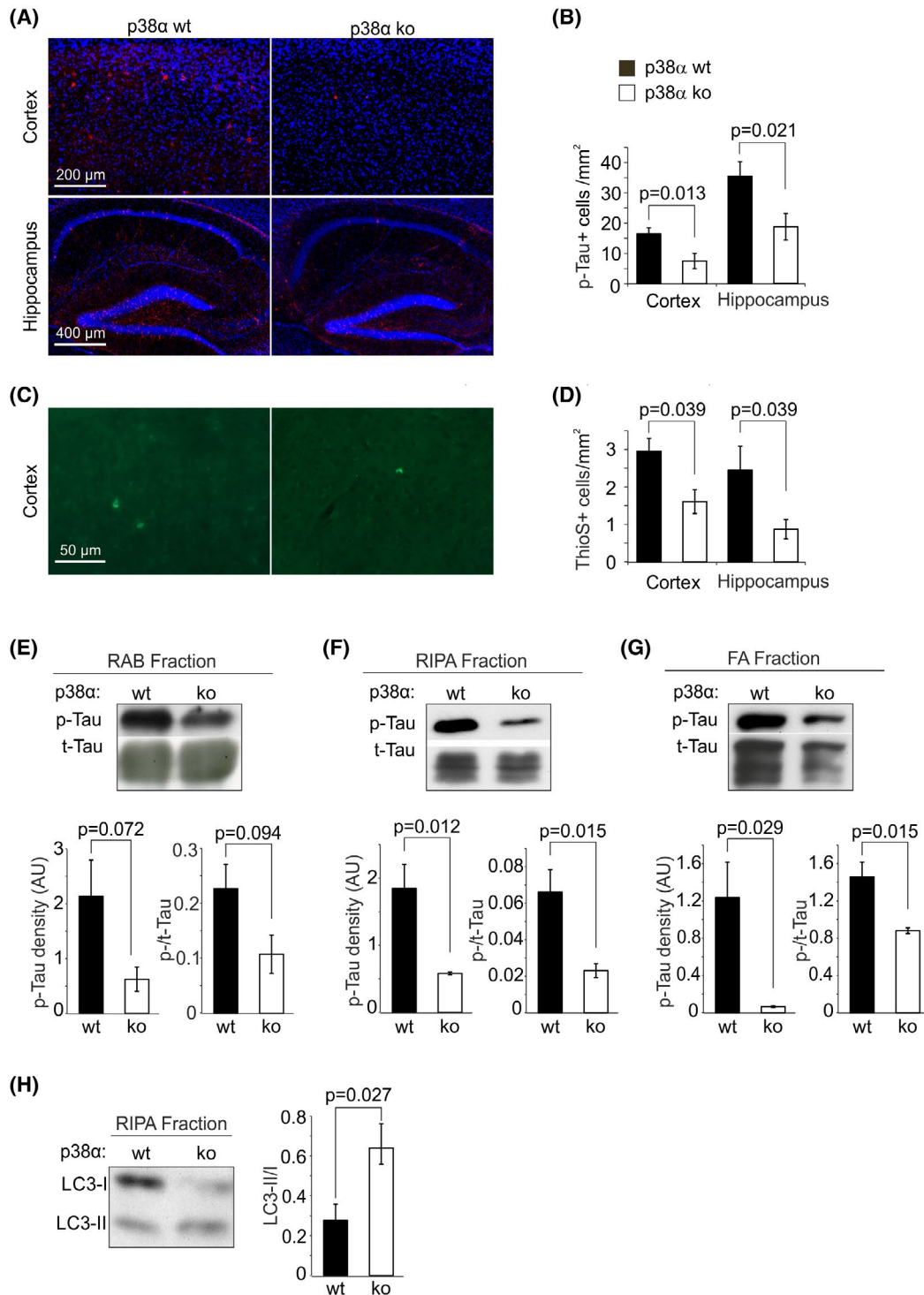


**FIGURE 9** Deletion of p38α-MAPK in neurons reduces p-Tau load in Tau-transgenic mice. Nine-month-old Tau-transgenic (tg) littermate mice with (ko) and without (wt) deletion of neuronal p38α-MAPK were analyzed for cerebral p-Tau load after immunofluorescent labeling with AT8 antibody (A) as well as for neurofibrillary tangles with thioflavine S (ThioS) staining (C). The p-Tau- or ThioS staining-positive cells were counted and adjusted by the relevant brain area. Deletion of p38α-MAPK in neurons significantly reduced the cerebral p-Tau-positive (B; *t* test; *n* = 8 per group) and ThioS staining-positive cells (D; *t* test; *n* ≥ 5 per group). Tau proteins were extracted from 9-month-old Tau<sup>tg</sup> mice with RAB, RIPA, and FA buffers and detected with Western blots for both phosphorylated and total Tau (p-Tau and t-Tau, respectively) (E-G). The protein levels of p-Tau are presented as both density (in arbitrary unit [AU]) and the ratio of p-/t-Tau. Deficiency of p38α-MAPK in neurons significantly reduces p-Tau proteins in RIPA and FA fractions, but not in RAB fraction (F and G; *t* test; *n* ≥ 4 per group). The RIPA fraction was further used to detect the autophagy marker LC3B-I and LC3B-II. Deletion of p38α-MAPK increased the ratio of LC3B-II/I (H; *t* test; *n* ≥ 6 per group)

further showed that p38 $\alpha$ -MAPK regulates calcium homeostasis. Especially the NMDA receptor-mediated calcium influx in neurons was affected, which might regulate neuronal plasticity and death in AD and in other neurodegenerative diseases.

Our previous study has shown that inhibition of p38 $\alpha$ -MAPK enhances autophagy in neurons, which promotes lysosomal degradation of BACE1.<sup>13</sup> As APP and C-terminal fragment of APP (C99) are also substrates of autophagy,<sup>48</sup> it is likely that p38 $\alpha$ -MAPK inhibition reduces A $\beta$  generation. Although we have not investigated p38 $\alpha$ -MAPK-deficient microglia, other studies have shown that inhibition of p38 $\alpha$ -MAPK potentially activates autophagy in macrophages.<sup>49</sup> Since autophagy both promotes the recycling of A $\beta$ -phagocytosing receptors CD36 and TREM2<sup>50</sup> and facilitates A $\beta$  degradation in microglia,<sup>51</sup> perhaps treatment with p38 $\alpha$ -MAPK inhibitor has the potential to degrade A $\beta$  in AD patients. We observed that deletion of neuronal p38 $\alpha$ -MAPK inhibits pro-inflammatory, but enhances anti-inflammatory activation in the brain of APP-transgenic mice. The inflammatory changes are likely secondary to the cerebral A $\beta$  reduction; however, provide a further protection for neurons.<sup>3</sup> Moreover, autophagy is an efficient mechanism to degrade p-Tau in the brain,<sup>28,52</sup> inhibition of p38 $\alpha$ -MAPK not only inhibits Tau phosphorylation<sup>15,53</sup> but should also increase p-Tau clearance in the AD brain. In Tau-transgenic mouse brain, we for the first time showed that deletion of p38 $\alpha$ -MAPK in neurons attenuates p-Tau protein. It was correlated with enhancement of autophagy. However, as t-Tau protein levels in the brain are not affected by neuronal p38 $\alpha$ -MAPK deficiency, the decrease of cerebral p-Tau is more likely due to the reduced phosphorylation of Tau proteins.

Furthermore, our study shows that phosphorylation of p38-MAPK is only increased in the brain but not in heart, liver and muscles in APP-transgenic mice, which corroborates the observation that p38-MAPK is locally activated at AD lesion sites in human brains.<sup>11,12</sup> Our careful evaluation indicates that deficiency of neuronal p38 $\alpha$ -MAPK does not affect the survival and cognitive function of APP-wild-type mice. Thus, inhibition of p38 $\alpha$ -MAPK might serve preventive and therapeutic effects against AD progress by targeting several key pathogenic mechanisms and limit its potential off-target actions.

Apart from its effects on autophagy, we observed that p38 $\alpha$ -MAPK regulates transcription of many calcium homeostasis-related genes in APP-transgenic mouse brain. Especially transcription and protein levels of NMDAR subunit NR2A (encoded by *grin2a* gene) are both downregulated in p38 $\alpha$ -deficient mouse brains. NMDAR mediates effects of the primary excitatory neurotransmitter glutamate. Under physiological condition, activation of NMDAR is essential for neuronal plasticity or long-term potentiation (LTP); however, under pathological conditions, such as in AD, NMDAR might increase calcium influx, which leads to excitotoxicity.<sup>54</sup>

A $\beta$  oligomers were reported to directly activate NMDARs, particularly NR2A-contained receptors.<sup>55</sup> A $\beta$  oligomers also block re-uptake of released glutamate from astrocytes and neurons, which leads to perisynaptic glutamate accumulation.<sup>56</sup> In APP-transgenic mouse brain, the level of resting calcium increases in neurites surrounding A $\beta$  deposits.<sup>57</sup> A $\beta$  oligomers-induced calcium overload in dendritic spines can be prevented by blocking NMDAR.<sup>44</sup> Memantine, as a NMDAR antagonist, has been proved to improve cognitive function and daily living of AD patients.<sup>58</sup> In our cultured neurons, deletion of p38 $\alpha$ -MAPK suppresses NMDA-induced calcium influx and neuronal apoptosis, which supports that inhibition of p38 $\alpha$ -MAPK protects neurons against calcium overload-induced neurotoxicity in AD.

Deletion of p38 $\alpha$ -MAPK also controls the neuronal excitotoxicity by regulating calcium buffering. In this study, we observed that p38 $\alpha$ -MAPK deficiency increased the gene expression of sodium/calcium exchanger 1 (Slc8a1) in APP<sup>tg</sup> mouse brain. Slc8a1 is located at plasma membranes, mitochondria, and endoplasmic reticulum (ER) of excitable cells, pumping cytoplasmic calcium out of cells or into calcium storage organelles.<sup>59</sup> Moreover, we detected reduced gene expression of sigma non-opioid intracellular receptor 1 (Sigmar1) in p38 $\alpha$ -MAPK-deficient mice. Sigmar1 resides at mitochondria-associated ER membrane, inhibiting store-operated calcium entry.<sup>60</sup> Inhibition of Sigmar1 was reported to attenuate cognitive deficits in an AD mouse model with intraventricle A $\beta$  injection.<sup>61</sup> In our cultured neurons, deletion of p38 $\alpha$ -MAPK enhances both glutamate-triggered calcium influx and the clearance of cytoplasmic calcium after glutamate removal. The rapid calcium clearance might compensate for the neurotoxic effects of elevated calcium level in p38 $\alpha$ -MAPK-deficient neurons. Thus, inhibition of p38 $\alpha$ -MAPK potentially protects neurons in AD brain by enhancing intracellular clearance of calcium, although the underlying mechanisms need to be further identified.

It should be noted that deletion of p38 $\alpha$ -MAPK increased L-glutamate-induced calcium influx, but decreased cytoplasmic calcium when cells were activated by NMDA. The increase of glutamate-induced calcium influx in p38 $\alpha$ -MAPK-deficient neurons is obviously mediated by non-NMDARs glutamate receptors, such as AMPA receptor, kainate receptors, and metabotropic-type glutamate receptors (mGluRs). In group 1 mGluRs activation-induced long-term depression (LTD), p38-MAPK activation initiates internalization of AMPA receptors at synapses.<sup>62</sup> Thus, p38 $\alpha$ -MAPK deficiency has the potential to preserve more AMPA receptors on the cell surface to facilitate the calcium entry. It is important to evaluate this possibility not only in cultured neurons but also in AD brain, as AMPA receptor-mediated calcium influx leads to synaptic dysfunction and neurodegeneration.<sup>63</sup>

Excitatory synapses contain AMPA and NMDA receptors, and mGluRs on dendritic spines. AMPA receptors

mediate most neuronal basal transmission. A $\beta$  treatments share the mechanisms with LTD to drive the endocytosis of synaptic AMPA receptors, which results in synaptic depression and dendritic spine loss.<sup>18</sup> Inhibition of neuronal p38 $\alpha$ -MAPK has the potential to inhibit A $\beta$ -induced LTD by blocking internalization of AMPA receptors.<sup>62</sup> Soluble A $\beta$  also impairs LTP by increasing the activity of extrasynaptic NMDARs. Inhibition of p38-MAPK has been observed to abolish A $\beta$ -caused inhibition of LTP in hippocampal slices.<sup>17</sup> We did not analyze electrophysiological activity of neurons in our AD mice; however, we observed that deficiency of neuronal p38 $\alpha$ -MAPK improves the cognitive function of APP-transgenic mice and prevents the loss of synaptic proteins. The preservation of matured mushroom spines that are enriched with AMPA receptors<sup>29</sup> further suggests protective effects of p38 $\alpha$ -MAPK deficiency on AMPA-mediated neuronal transmission in APP-transgenic mice. Moreover, our transcriptome analysis shows that the transcription of *grial*, which encodes AMPA receptor subunit 1, is upregulated in the brain of neuronal p38 $\alpha$ -MAPK-deficient APP-transgenic mice (see Table S1). Thus, inhibition of neuronal p38-MAPK potentially improves synaptic plasticity in AD brain.

Our study shows that p38 $\alpha$ -MAPK deficiency protects neuron in AD pathogenesis. However, physiological functions of p38-MAPK still need to be noted; for example, p38 $\alpha$ -MAPK is essential in erythropoiesis.<sup>64</sup> In our AD mice, neuronal p38 $\alpha$ -MAPK was deleted from the birth. Our results indicate more preventive than therapeutic effects of p38 $\alpha$ -MAPK inhibition in AD.

In the last decades, many clinical interventions, especially A $\beta$  immunization,<sup>65</sup> have been attempted to reduce cerebral A $\beta$ . Unfortunately, none of them resulted in efficacious therapies for AD patients. Our study demonstrated that deficiency of neuronal p38 $\alpha$ -MAPK ameliorates AD-associated brain pathology in both APP and Tau-transgenic animal models. As potential mechanisms, inhibition of neuronal p38 $\alpha$ -MAPK not only reduces generation of A $\beta$  and p-Tau, but also protects neurons by preventing calcium overload. Our studies support p38 $\alpha$ -MAPK as a novel target for AD therapy, although further studies are required.

## ACKNOWLEDGMENTS

We thank Dr M. Jucker (Hertie Institute for Clinical Brain Research, Tübingen) for providing APP-transgenic mice; and Dr K. Nave (Max-Planck-Institute for Medicine, Göttingen) for Nex-Cre mice. The floxed-p38 $\alpha$ -MAPK (p38 $\alpha$ fl/fl) mice were kindly provided by Dr K. Otsu (Osaka University) through the RIKEN Bioresource Center. We appreciate Mirjam Göttel for her excellent technical assistance. This work was supported by 'Deutsche Forschungsgemeinschaft (LI1725/2-1; to YL), HOMFORexcell program (to LS), and German Federal

Ministry of Research and Education grant for de.NBI (031L0101D; to KN).

## CONFLICT OF INTEREST

The authors declare that they have no conflicts of interest with the contents of this article.

## AUTHOR CONTRIBUTIONS

L. Schnöder and Y. Liu designed research; L. Schnöder, G. Gasparoni, A. Schottek, I. Tomic, and A. Christmann performed experiments; L. Schnöder, G. Gasparoni, and K. Nordström analyzed data; L. Schnöder and Y. Liu wrote the paper; K. Fassbender, J. Walter, and K.H. Schäfer contributed analytic tools; M.D. Menger provided animal facility. Y. Liu coordinated the whole study. All authors read and approved the final manuscript.

## REFERENCES

1. Querfurth HW, LaFerla FM. Alzheimer's disease. *N Engl J Med.* 2010;362:329-344.
2. Mucke L, Selkoe DJ. Neurotoxicity of amyloid beta-protein: synaptic and network dysfunction. *Cold Spring Harb Perspect Med.* 2012;2:a006338.
3. Wyss-Coray T, Rogers J. Inflammation in Alzheimer disease—a brief review of the basic science and clinical literature. *Cold Spring Harb Perspect Med.* 2012;2:a006346.
4. Ghosh S, Wu MD, Shaftel SS, et al. Sustained interleukin-1beta overexpression exacerbates tau pathology despite reduced amyloid burden in an Alzheimer's mouse model. *J Neurosci.* 2013;33:5053-5064.
5. Ryan SD, Whitehead SN, Swayne LA, et al. Amyloid-beta42 signals tau hyperphosphorylation and compromises neuronal viability by disrupting alkylacylglycerophosphocholine metabolism. *Proc Natl Acad Sci U S A.* 2009;106:20936-20941.
6. Maphis N, Xu G, Kokiko-Cochran ON, et al. Reactive microglia drive tau pathology and contribute to the spreading of pathological tau in the brain. *Brain.* 2015;138:1738-1755.
7. Shimada H, Kitamura S, Shinotoh H, et al. Association between Abeta and tau accumulations and their influence on clinical features in aging and Alzheimer's disease spectrum brains: a [11C] PBB3-PET study. *Alzheimers Dement (Amst).* 2017;6:11-20.
8. Haass C, Kaether C, Thinakaran G, Sisodia S. Trafficking and proteolytic processing of APP. *Cold Spring Harb Perspect Med.* 2012;2:a006270.
9. Egan MF, Kost J, Tariot PN, et al. Randomized trial of veru-becestat for mild-to-moderate Alzheimer's disease. *N Engl J Med.* 2018;378:1691-1703.
10. Lahiri DK, Maloney B, Long JM, Greig NH. Lessons from a BACE1 inhibitor trial: off-site but not off base. *Alzheimers Dement.* 2014;10:S411-S419.
11. Hensley K, Floyd RA, Zheng NY, et al. p38 kinase is activated in the Alzheimer's disease brain. *J Neurochem.* 1999;72:2053-2058.
12. Sun A, Liu M, Nguyen XV, Bing G. P38 MAP kinase is activated at early stages in Alzheimer's disease brain. *Exp Neurol.* 2003;183:394-405.
13. Schnöder L, Hao W, Qin Y, et al. Deficiency of neuronal p38 $\alpha$ -MAPK attenuates amyloid pathology in Alzheimer disease

- mouse and cell models through facilitating lysosomal degradation of BACE1. *J Biol Chem.* 2016;291:2067-2079.
14. Bachstetter AD, Xing B, de Almeida L, Dimayuga ER, Watterson DM, Van Eldik LJ. Microglial p38alpha MAPK is a key regulator of proinflammatory cytokine up-regulation induced by toll-like receptor (TLR) ligands or beta-amyloid (Abeta). *J Neuroinflammation.* 2011;8:79.
  15. Reynolds CH, Nebreda AR, Gibb GM, Utton MA, Anderton BH. Reactivating kinase/p38 phosphorylates tau protein in vitro. *J Neurochem.* 1997;69:191-198.
  16. Zhu X, Rottkamp CA, Boux H, Takeda A, Perry G, Smith MA. Activation of p38 kinase links tau phosphorylation, oxidative stress, and cell cycle-related events in Alzheimer disease. *J Neuropathol Exp Neurol.* 2000;59:880-888.
  17. Li S, Jin M, Koeglsperger T, Shepardson NE, Shankar GM, Selkoe DJ. Soluble Abeta oligomers inhibit long-term potentiation through a mechanism involving excessive activation of extrasynaptic NR2B-containing NMDA receptors. *J Neurosci.* 2011;31:6627-6638.
  18. Hsieh H, Boehm J, Sato C, et al. AMPAR removal underlies Abeta-induced synaptic depression and dendritic spine loss. *Neuron.* 2006;52:831-843.
  19. Scheltens P, Prins N, Lammertsma A, et al. An exploratory clinical study of p38alpha kinase inhibition in Alzheimer's disease. *Ann Clin Transl Neurol.* 2018;5:464-473.
  20. Bachstetter AD, Norris CM, Sompol P, et al. Early stage drug treatment that normalizes proinflammatory cytokine production attenuates synaptic dysfunction in a mouse model that exhibits age-dependent progression of Alzheimer's disease-related pathology. *J Neurosci.* 2012;32:10201-10210.
  21. Munoz L, Ralay Ranaivo H, Roy SM, et al. A novel p38 alpha MAPK inhibitor suppresses brain proinflammatory cytokine up-regulation and attenuates synaptic dysfunction and behavioral deficits in an Alzheimer's disease mouse model. *J Neuroinflammation.* 2007;4:21.
  22. Maphis N, Jiang S, Xu G, et al. Selective suppression of the alpha isoform of p38 MAPK rescues late-stage tau pathology. *Alzheimers Res Ther.* 2016;8:54.
  23. Colie S, Sarroca S, Palenzuela R, et al. Neuronal p38alpha mediates synaptic and cognitive dysfunction in an Alzheimer's mouse model by controlling beta-amyloid production. *Sci Rep.* 2017;7:45306.
  24. Radde R, Bolmont T, Kaeser SA, et al. Abeta42-driven cerebral amyloidosis in transgenic mice reveals early and robust pathology. *EMBO Rep.* 2006;7:940-946.
  25. Nishida K, Yamaguchi O, Hirotsu S, et al. p38alpha mitogen-activated protein kinase plays a critical role in cardiomyocyte survival but not in cardiac hypertrophic growth in response to pressure overload. *Mol Cell Biol.* 2004;24:10611-10620.
  26. Goebbels S, Bormuth I, Bode U, Hermanson O, Schwab MH, Nave KA. Genetic targeting of principal neurons in neocortex and hippocampus of NEX-Cre mice. *Genesis.* 2006;44:611-621.
  27. Yoshiyama Y, Higuchi M, Zhang B, et al. Synapse loss and microglial activation precede tangles in a P301S tauopathy mouse model. *Neuron.* 2007;53:337-351.
  28. Qin Y, Liu Y, Hao W, et al. Stimulation of TLR4 attenuates Alzheimer's disease-related symptoms and pathology in Tau-transgenic mice. *J Immunol.* 2016;197:3281-3292.
  29. Berry KP, Nedivi E. Spine dynamics: are they all the same? *Neuron.* 2017;96:43-55.
  30. Liu Y, Liu X, Hao W, et al. IKKbeta deficiency in myeloid cells ameliorates Alzheimer's disease-related symptoms and pathology. *J Neurosci.* 2014;34:12982-12999.
  31. DeVos SL, Miller RL, Schoch KM, et al. Tau reduction prevents neuronal loss and reverses pathological tau deposition and seeding in mice with tauopathy. *Sci Transl Med.* 2017;9:eaag0481.
  32. Martin M. Cutadapt removes adapter sequences from high-throughput sequencing reads. *EMBnet.J.* 2011;17:3.
  33. Dobin A, Davis CA, Schlesinger F, et al. STAR: ultrafast universal RNA-seq aligner. *Bioinformatics.* 2013;29:15-21.
  34. Li B, Dewey CN. RSEM: accurate transcript quantification from RNA-Seq data with or without a reference genome. *BMC Bioinform.* 2011;12:323.
  35. Soneson C, Love MI, Robinson MD. Differential analyses for RNA-seq: transcript-level estimates improve gene-level inferences. *F1000Res.* 2015;4:1521.
  36. Robinson MD, McCarthy DJ, Smyth GK. edgeR: a bioconductor package for differential expression analysis of digital gene expression data. *Bioinformatics.* 2010;26:139-140.
  37. Luo W, Brouwer C. Pathview: an R/Bioconductor package for pathway-based data integration and visualization. *Bioinformatics.* 2013;29:1830-1831.
  38. Luo W, Friedman MS, Shedden K, Hankenson KD, Woolf PJ. GAGE: generally applicable gene set enrichment for pathway analysis. *BMC Bioinform.* 2009;10:161.
  39. Luo W, Pant G, Bhavnasi YK, Blanchard SG, Jr., Brouwer C. Pathview Web: user friendly pathway visualization and data integration. *Nucleic Acids Res.* 2017;45:W501-W508.
  40. Sheng JG, Jones RA, Zhou XQ, et al. Interleukin-1 promotion of MAPK-p38 overexpression in experimental animals and in Alzheimer's disease: potential significance for tau protein phosphorylation. *Neurochem Int.* 2001;39:341-348.
  41. Shi Y. Mechanistic insights into precursor messenger RNA splicing by the spliceosome. *Nat Rev Mol Cell Biol.* 2017;18:655-670.
  42. Nuzzo D, Inguglia L, Walters J, Picone P, Di Carlo M. A shotgun proteomics approach reveals a new toxic role for Alzheimer's disease Abeta peptide: spliceosome impairment. *J Proteome Res.* 2017;16:1526-1541.
  43. Franzén O, Gan LM, Björkegren JLM. PPanglaoDB: a web server for exploration of mouse and human single-cell RNA sequencing data. *Database (Oxford).* 2019;2019:baz046. doi:10.1093/database/baz046.
  44. Arbel-Ornath M, Hudry E, Boivin JR, et al. Soluble oligomeric amyloid-β induces calcium dyshomeostasis that precedes synapse loss in the living mouse brain. *Mol Neurodegener.* 2017;12:27.
  45. Green KN, LaFerla FM. Linking calcium to Abeta and Alzheimer's disease. *Neuron.* 2008;59:190-194.
  46. Ittner LM, Ke YD, Delerue F, et al. Dendritic function of tau mediates amyloid-beta toxicity in Alzheimer's disease mouse models. *Cell.* 2010;142:387-397.
  47. Vossel KA, Zhang K, Brodbeck J, et al. Tau reduction prevents Abeta-induced defects in axonal transport. *Science.* 2010;330:198.
  48. Parr C, Carzaniga R, Gentleman SM, Van Leuven F, Walter J, Sastre M. Glycogen synthase kinase 3 inhibition promotes lysosomal biogenesis and autophagic degradation of the amyloid-beta precursor protein. *Mol Cell Biol.* 2012;32:4410-4418.
  49. Keil E, Hocker R, Schuster M, et al. Phosphorylation of Atg5 by the Gadd45beta-MEKK4-p38 pathway inhibits autophagy. *Cell Death Differ.* 2013;20:321-332.

50. Lucin KM, O'Brien CE, Bieri G, et al. Microglial beclin 1 regulates retromer trafficking and phagocytosis and is impaired in Alzheimer's disease. *Neuron*. 2013;79:873-886.
51. Cho MH, Cho K, Kang HJ, et al. Autophagy in microglia degrades extracellular beta-amyloid fibrils and regulates the NLRP3 inflammasome. *Autophagy*. 2014;10:1761-1775.
52. Inoue K, Rispoli J, Kaphzan H, et al. Macroautophagy deficiency mediates age-dependent neurodegeneration through a phospho-tau pathway. *Mol Neurodegener*. 2012;7:48.
53. Li Y, Liu L, Barger SW, Griffin WS. Interleukin-1 mediates pathological effects of microglia on tau phosphorylation and on synaptophysin synthesis in cortical neurons through a p38-MAPK pathway. *J Neurosci*. 2003;23:1605-1611.
54. Cotman CW, Monaghan DT, Ganong AH. Excitatory amino acid neurotransmission: NMDA receptors and Hebb-type synaptic plasticity. *Annu Rev Neurosci*. 1988;11:61-80.
55. Texido L, Martin-Satue M, Alberdi E, Solsona C, Matute C. Amyloid beta peptide oligomers directly activate NMDA receptors. *Cell Calcium*. 2011;49:184-190.
56. Zott B, Simon MM, Hong W, et al. A vicious cycle of beta amyloid-dependent neuronal hyperactivation. *Science*. 2019;365:559-565.
57. Kuchibhotla KV, Goldman ST, Lattarulo CR, Wu HY, Hyman BT, Bacskai BJ. Abeta plaques lead to aberrant regulation of calcium homeostasis in vivo resulting in structural and functional disruption of neuronal networks. *Neuron*. 2008;59:214-225.
58. Reisberg B, Doody R, Stöffler A, et al. Memantine in moderate-to-severe Alzheimer's disease. *N Engl J Med*. 2003;348:1333-1341.
59. Khananshvili D. The SLC8 gene family of sodium-calcium exchangers (NCX)—structure, function, and regulation in health and disease. *Mol Aspects Med*. 2013;34:220-235.
60. Srivats S, Balasuriya D, Pasche M, et al. Sigma1 receptors inhibit store-operated Ca<sup>2+</sup> entry by attenuating coupling of STIM1 to Orai1. *J Cell Biol*. 2016;213:65-79.
61. Yin J, Sha S, Chen T, et al. Sigma-1 (sigma(1)) receptor deficiency reduces beta-amyloid(25–35)-induced hippocampal neuronal cell death and cognitive deficits through phosphorylation of the NMDA receptor NR2B. *Neuropharmacology*. 2015;89:215-224.
62. Eales KL, Palygin O, O'Loughlin T, et al. The MK2/3 cascade regulates AMPAR trafficking and cognitive flexibility. *Nat Commun*. 2014;5:4701.
63. Whitehead G, Regan P, Whitcomb DJ, Cho K. Ca(2+)-permeable AMPA receptor: a new perspective on amyloid-beta mediated pathophysiology of Alzheimer's disease. *Neuropharmacology*. 2017;112:221-227.
64. Tamura K, Sudo T, Senftleben U, Dadak AM, Johnson R, Karin M. Requirement for p38alpha in erythropoietin expression: a role for stress kinases in erythropoiesis. *Cell*. 2000;102:221-231.
65. Doody RS, Thomas RG, Farlow M, et al. Phase 3 trials of solanezumab for mild-to-moderate Alzheimer's disease. *N Engl J Med*. 2014;370:311-321.

## SUPPORTING INFORMATION

Additional supporting information may be found online in the Supporting Information section.

**How to cite this article:** Schnöder L, Gasparoni G, Nordström K, et al. Neuronal deficiency of p38 $\alpha$ -MAPK ameliorates symptoms and pathology of APP or Tau-transgenic Alzheimer's mouse models. *The FASEB Journal*. 2020;34:9628–9649. <https://doi.org/10.1096/fj.201902731RR>